*Physics – Uspekhi* **47** (1) 69 – 98 (2004) 

*REVIEWS OF TOPICAL PROBLEMS* PACS numbers: 42.65.Ky, 42.65.Dr, 42.65.Re, 42.65.Wi

# Nonlinear optics of microstructure fibers

A M Zheltikov

DOI: 10.1070/PU2004v047n01ABEH001731

## Contents



**Abstract. Microstructure fibers have opened a new phase in nonlinear optics. Due to their unique properties, fibers of this type radically enhance all the basic nonlinear-optical phenomena, offering new strategies for frequency conversion, spectral transformation, and control of ultrashort laser pulses. These fibers allow supercontinuum radiation to be efficiently generated using nano- and subnanojoule femtosecond pulses. Here, we analyze the physical mechanisms behind the enhancement of nonlinear-optical interactions of ultrashort pulses in microstructure and hollow photonic-crystal fibers and discuss applications of microstructure fibers for highly efficient supercontinuum generation and frequency conversion of femtosecond laser pulses.**

**A M Zheltikov** International Laser Center; Physics Department, M V Lomonosov Moscow State University
Vorob'evy gory, 119992 Moscow, Russian Federation
Tel. (7-095) 939 51 74
Fax: (7-095) 939 31 13
E-mail: zheltikov@top.phys.msu.su

Received 20 August 2003, revised 6 September 2003
*Uspekhi Fizicheskikh Nauk* **174** (1) 73 – 105 (2004)
Translated by A M Zheltikov; edited by M V Chekhova

## 1. Introduction

Optical fibers are changing their structure. Fibers of a new architecture — microstructure (MS) fibers — are emerging as a powerful tool supplementing conventional fibers in optical physics, biomedicine, and photochemistry. Guided modes of electromagnetic radiation are formed in these fibers as a result of the interference of waves scattered and reflected from microinhomogeneities in the refractive index profile. Microstructure fibers lead to revolutionary changes in optical metrology, nonlinear optics, laser physics, and ultrafast photonics. The impressive progress in several fields of basic science and applied research that has become possible in the past few years due to the use of MS fibers has made these fibers one of the most significant achievements in optical technologies within the last decade.

The generic idea of microstructure fibers is illustrated in Fig. 1. In contrast to conventional optical fibers (Fig. 1a), which consist [1, 2] of a core with the refractive index $n_{\rm core}$ and a cladding with the refractive index $n_{\rm clad}$, MS fibers guide electromagnetic radiation through a fused silica or glass microstructure with periodic or aperiodic air holes (Fig. 1b). Fabrication of such a microstructure typically involves drawing a preform consisting of an array of capillaries at a high temperature.

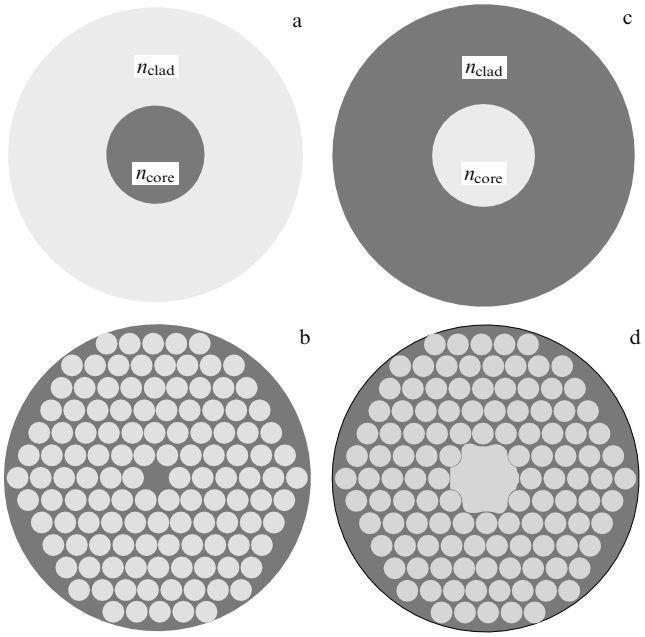


**Figure 1.** Optical fibers of various architectures: (a) standard optical fiber, consisting of a core with the refractive index $n_{core}$ and a cladding with the refractive index $n_{clad} < n_{core}$; (b) microstructure fiber; (c) standard hollow fiber with a solid cladding, $n_{core} < n_{clad}$; and (d) hollow-core fiber with a photonic-crystal cladding. Dark areas correspond to a material with a higher refractive index.

A defect in this microstructure, formed by one or several missing air holes (at the center of the structure in Fig. 1b), may guide the light in a similar way to the core in a standard fiber. The inequality $n_{clad} < n_{core}$ ensures total internal reflection in standard fibers. Guided modes of MS fibers originate from the interference of reflected and scattered waves. With an effective refractive index $n_{eff}$ defined for a microstructure fiber cladding, the condition for the existence of guided modes in the MS-fiber core, formed by a defect in a glass – air or fused silica – air microstructure (Fig. 1b), is written similarly to the condition of total internal reflection in a standard fiber, $n_{eff} < n_{core}$.

Along with conventional waveguiding regimes, supported by total internal reflection, MS fibers can, under certain conditions, guide electromagnetic radiation due to the high reflectivity of the fiber cladding within photonic band gaps. Such regimes of waveguiding can be implemented in fibers with a two-dimensionally periodic microstructure cladding (a two-dimensional photonic crystal) and a hollow core (Fig. 1d).

Photonic band gaps arising in the transmission spectrum of a two-dimensionally periodic cladding in fibers of this type provide high reflection coefficients for radiation propagating along the hollow core, radically reducing optical losses, which are typical of air-guided modes in hollow fibers (Fig. 1c) and which rapidly grow with a decrease in the core diameter of a hollow fiber.

Technologically, the possibility of fabricating simple microstructure fibers was demonstrated back in the early 1970s. One of the first MS fibers fabricated by Bell Labs [3] had a fused silica cobweb core bounded by a solid fused silica

**Table 1.** Catalogue of microstructure fibers: design, technology, properties, and applications.

| Fiber type | Fiber structure | Mechanism of waveguiding | Applications | | | | | |
|---|---|---|---|---|---|---|---|---|
| | | | Telecommunications | Metrology | Ultrafast photonics | Nonlinear optics | Laser physics | Biomedicine and photochemistry |
| MS fibers with a fused silica or glass solid core [4, 9] | 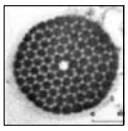 | Total internal reflection | Acceptable level of losses has been achieved | Octave-spanning frequency combs for femtosecond clock | Pulse compression, phase measurements, CEO and GVD control, solitons | Enhanced SPM, XPM, FWM, THG, SRS, and SC generation | New fiber lasers | Optical coherence tomography |
| Hollow-core PCFs [38, 40] | 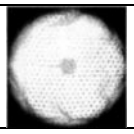 | Photonic band gaps of the PCF cladding | Losses have to be reduced | | Transportation of short pulses | Enhanced SRS, FWM, and SPM | | Transmission of laser pulses for laser dentistry |
| MS-integrated arrays of waveguide channels [33, 123] | 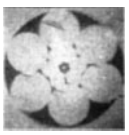 | Total internal reflection | Multiplex frequency conversion | | GVD control, solitons | Pump-depleting FWM | Highly efficient frequency conversion of femtosecond pulses | Photochromism initiation |
| Tapered fibers [51, 52] | 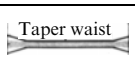 Taper waist | Total internal reflection | Couplers, multiplexers, demultiplexers | Octave-spanning frequency combs for femtosecond clock | GVD control, solitons | Enhanced SPM, FWM, THG, and SC generation; multiple phase-matched cascaded FWM | New fiber lasers | Optical coherence tomography |

*Notation*: MS fiber, microstructure fiber; PCF, photonic-crystal fiber; GVD, group-velocity dispersion; CEO, carrier-envelope frequency offset; SPM, self-phase modulation; XPM, cross-phase modulation; FWM, four-wave mixing; THG, third-harmonic generation; SRS, stimulated Raman scattering; SC, supercontinuum.

cladding. It was not, however, until much later that the wealth of functional capabilities of MS fibers was understood on the basis of conceptual and technological progress in several areas of optics and laser physics, including ultrafast photonics and optics of periodic structures, photonic crystals, and random media.

The modern phase in the optics of microstructure fibers was opened by the seminal work of Philip Russell and his group, published in 1996 [4]. This first publication demonstrated that fused silica fibers with an array of air holes running along the cladding parallel to the fiber core can support single-mode waveguiding within a remarkably broad frequency range.

Intense studies, stimulated by the pioneering work of Russell's group, have revealed several unique properties of microstructure fibers and have resulted in the observation of new physical phenomena in fibers of this type [5–11]. Microstructure fibers offer new solutions for laser physics, photonics, and optical technologies (see Table 1), as they combine dispersion tunability and a high degree of light-field confinement in the fiber core. Dispersion of such fibers is tailored by changing their core–cladding geometry [12, 13], while a strong light-field confinement is due to the high refractive-index step between the core and the MS cladding [14, 15]. Controlled dispersion of MS fibers is the key to new solutions in optical telecommunications and ultrafast photonics. The high degree of light-field confinement, on the other hand, radically enhances the whole catalogue of nonlinear-optical processes.

Several classes of MS fibers have been developed to meet the demands of basic science and applied research (see Fig. 2a). The cross-section view of a generic-type MS fiber is shown in the first row of Table 1. An array of air holes in the MS cladding of the fiber is not necessarily periodic. Guided modes in such a fiber are supported, similarly to standard fibers, by total internal reflection from the core–cladding interface, with the effective refractive index of the MS cladding being lower than the refractive index of the core due to the presence of air holes in the cladding.

The confinement of electromagnetic radiation and the fraction of laser power guided along the fiber core are controlled in the case of such an MS fiber by varying the air-filling fraction of the cladding and the ratio of the core diameter to the radiation wavelength [15]. Microstructure fibers of this type enhance a broad class of nonlinear-optical processes [5], including self-phase modulation (SPM) and cross-phase modulation (XPM) [15, 16], four-wave mixing (FWM) [17–21], third-harmonic generation [16, 22], and stimulated Raman scattering (SRS) [17].

Enhancement of nonlinear-optical interactions and controlled dispersion of guided modes in MS fibers allow supercontinuum radiation, i.e., white-light emission with a broad continuous spectrum (Fig. 2b), to be generated [5, 23–26] using low-energy maser pulses, including unamplified femtosecond pulses. Supercontinuum emission with spectra spanning over several octaves can often be produced with MS fibers. Supercontinuum-generating MS fibers result in revolutionary changes in optical metrology [27–31] and are widely employed in laser biomedicine [32], spectroscopy [33], photochemistry [34], and ultrafast optics [35, 36].

Dispersion control of guided modes in microstructure fibers offers new solutions to the phase-matching problem in nonlinear optics [17–21], allowing MS fibers to be employed not only as sources of broadband emission but also as

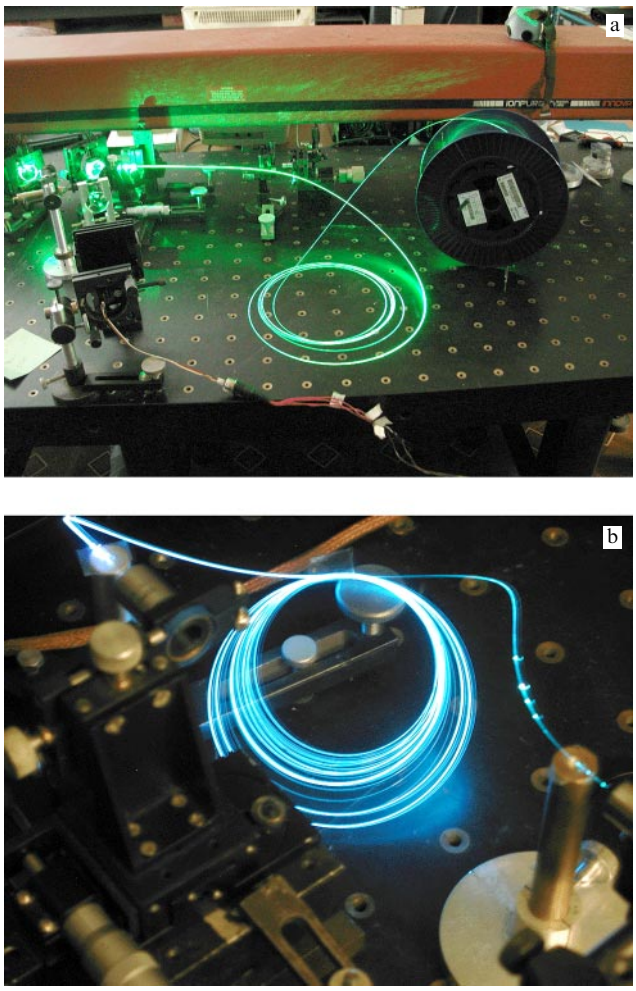


**Figure 2.** (a) Microstructure fibers in a laser experiment. (b) Supercontinuum generation by unamplified Ti:sapphire-laser pulses in microstructure fibers. Experiments were performed at the Laboratory of Photonics and Nonlinear Spectroscopy, Chair of General Physics and Wave Processes, Physics Department, M V Lomonosov Moscow State University. The fibers were fabricated by the group of Professor Yu N Kondrat'ev (S I Vavilov State Optical Institute).

efficient frequency converters for ultrashort laser pulses. The size of the waveguiding channel in an MS fiber is the key parameter controlling the dispersion properties of guided modes in such structures. Arrays of threadlike submicron fused silica channels microstructure-integrated in an MS fiber can, therefore, function as multiplex frequency upconverters, providing high-efficiency nonlinear-optical spectral transformation even in the case of nano- and subnanojoule ultrashort laser pulses [37].

Air holes periodically arranged in the cladding of hollow-core MS fibers [38–40] support air-guided modes in such fibers (the second row in Table 1). The key property of two-dimensionally periodic structures (two-dimensional photonic crystals) is the existence of photonic band gaps in their transmission and dispersion. Within these frequency ranges, the periodic structure becomes highly reflective, as the electromagnetic field cannot exist in the form of Bloch waves propagating inside the photonic crystal.

Hollow photonic-crystal fibers (PCFs) offer unique possibilities for enhanced nonlinear-optical interactions in the gas phase, as recently demonstrated by experiments on stimulated Raman scattering [41], four-wave mixing [42], and

self-phase modulation [43]. Hollow PCFs can also be employed for laser guiding of microparticles and atoms [44], as well as for the transportation of high-power laser radiation in laser technologies for material microprocessing and micromachining [45] and laser biomedicine [46].

Microstructure fibers with coupled waveguide channels in the form of an array around the central fiber core (the third row in Table 1) or in the form of a cobweb bounded by a solid cladding are ideally suited for controlled spectral transformation of ultrashort pulses and supercontinuum generation [19, 20, 47, 48]. Such fibers also provide deeper insights into fundamental aspects related to the interaction of laser radiation with micro- and nanostructured matter, and shed light on the influence of disorder in the fiber cladding on the properties of air-guided modes in the core of hollow PCFS [49].

Tapered fibers are also classified here as microstructure fibers (the last row in Table 1). Tapered fibers are employed more and more intensely for nonlinear-optical spectral transformation of ultrashort laser pulses and supercontinuum generation. Enhancement of nonlinear-optical processes in such fibers was experimentally demonstrated by Stegeman's group in the early 1990s [50]. Recent experiments [51, 52] have shown that tapered fibers can generate supercontinuum emission with a spectral width of one or two octaves starting with the nanojoule level of initial energies of femtosecond laser pulses. Similarly to white-light generation in MS fibers, supercontinuum emission from tapered fibers is actively employed in optical metrology [30], spectroscopy [53], ultrafast optics [54], and laser biomedicine [55].

The taper-waist region of tapered fibers is typically characterized by a high refractive-index step between the core (which is usually made of fused silica) and the cladding (air), providing a high degree of light confinement in the fiber core. The wavelength corresponding to zero group-velocity dispersion can be tuned within virtually the entire visible range by changing the taper-waist diameter. The second point of zero group-velocity dispersion [51], which exists for tapered fibers with a sufficiently small taper-waist diameter, is an interesting new feature, which holds much promise for enhanced nonlinear optics and the creation of tapered-fiber lasers [56].

Table 1 briefly summarizes the main recent achievements in the optics of microstructure fibers. In this review, we will examine the basic physical mechanisms behind the enhancement of nonlinear-optical processes in microstructure and hollow photonic-crystal fibers and discuss the results of experiments demonstrating highly efficient supercontinuum generation and frequency upconversion of ultrashort pulses in fibers of these types.

## 2. Waveguide enhancement of nonlinear-optical processes in microstructure fibers

In this section, we will explore the ways to achieve the limiting waveguide enhancement of nonlinear-optical processes in microstructure and photonic-crystal fibers. The waveguide enhancement of nonlinear-optical processes will be shown to be physically limited because of the competition of diffraction and refractive-index-step radiation confinement. We will demonstrate that, in the case of the limiting refractive-index steps for fused silica fibers, the maximum waveguide enhancement of nonlinear-optical processes is achieved with submicron fiber core diameters. The maximum waveguide enhancement of coherent anti-Stokes Raman scattering (CARS) in a hollow microstructure fiber relative to the regime of tight focusing will be shown to scale as $\lambda^2/\alpha^2 a^4$ with radiation wavelength $\lambda$, inner fiber radius $a$, and magnitude of radiation losses $\alpha$.

### 2.1 Microstructure fibers and a new phase in nonlinear optics

The advent of microstructure and photonic-crystal fibers [4–11] has opened a new phase in the nonlinear optics of guided waves. Such fibers provide a strong confinement of electromagnetic radiation in the fiber core [14, 15] and offer many degrees of freedom in dispersion tailoring through variations in the core–cladding geometry of the fiber [12, 13]. Due to their unique properties, microstructure and photonic-crystal fibers enhance the whole catalogue of nonlinear-optical processes, making nonlinear optics accessible to unamplified femtosecond laser pulses and suggesting new solutions for the frequency conversion and spectral transformation of ultrashort laser pulses, as well as for the phase and temporal control of such pulses [7].

The enhancement of a broad class of nonlinear-optical phenomena, including self-phase modulation [15], four-wave mixing and parametric processes [17–20], third-harmonic generation [16, 22], stimulated Raman scattering [17, 18], and soliton formation [25], leads to an efficient generation of radiation with a very broad continuous spectrum — supercontinuum [23, 24]. Supercontinuum generation in microstructure fibers is the backbone of femtosecond systems for high-precision measurements [27–31]. This phenomenon also holds much promise for the measurement and control of the phase of ultrashort pulses [35] and has broad applications in ultrafast photonics [36], spectroscopy [33], and biomedical optics [32].

Supercontinuum generation is, on the other hand, a result of a complicated interplay between many nonlinear-optical processes, providing deeper insights into the basics of nonlinear optics and leading to spectacular phenomena and new interesting manifestations of nonlinear-optical interactions. Physical scenarios of supercontinuum generation in microstructure fibers suggest an exciting subject for basic research in the interdisciplinary area of ultrafast nonlinear optics and the physics of micro- and nanostructures.

Fibers with a cladding in the form of a two-dimensionally periodic microstructure (two-dimensional photonic crystal) and a hollow core, first demonstrated by Cregan et al. [38], are one of the most interesting and promising types of microstructure fibers. Photonic band gaps in the transmission spectrum of a two-dimensional periodic cladding in these fibers provide high reflection coefficients for electromagnetic radiation propagating along the hollow core of the fiber, allowing a specific regime of waveguiding to be implemented [38–40]. This mechanism of waveguiding is of special interest for telecommunication applications, opening, at the same time, ways to enhance nonlinear-optical processes.

Benabid et al. [41] have recently demonstrated a radical enhancement of stimulated Raman scattering in hollow-core photonic-crystal fibers. Such fibers can also be employed for laser manipulation of small-size particles [44]. The structure of hollow-core photonic-crystal fibers is ideally suited for the transportation of high-power laser radiation [45], high-order harmonic generation [58], transmission of ultrashort laser pulses [59], and fiber-optic delivery of laser radiation in technological laser systems [45].

In view of the exciting possibilities offered by microstructure and hollow-core photonic-crystal fibers in nonlinear optics, the physical factors determining the limiting efficiencies of nonlinear-optical processes in such fibers are of special interest. Understanding these factors would allow a strategy for optimizing the structure and parameters of MS and hollow-core photonic-crystal fibers to be developed for the maximum enhancement of nonlinear-optical processes.

Such analysis is the main task of this review. We will consider the processes of stimulated Raman scattering (SRS) and coherent anti-Stokes Raman scattering in hollow-core photonic-crystal fibers, examine the factors determining the limiting SRS and CARS efficiencies in such fibers, and find the optimal fiber lengths for SRS and CARS processes, taking into consideration waveguide losses, as well as group-delay and phase-mismatch effects.

We will show that microstructure fibers open the way to achieving the maximum waveguide enhancement of nonlinear-optical processes. Physically, the existence of this maximum for waveguide enhancement is associated with a competition between diffraction and radiation confinement in a waveguide due to the refractive-index step. We will derive asymptotic expressions providing in several important cases an adequate qualitative description of the waveguide enhancement of nonlinear-optical processes and allowing the optimal fiber core diameters for the maximum enhancement of nonlinear-optical interactions to be estimated with satisfactory accuracy.

### 2.2 The physics behind the waveguide enhancement of nonlinear-optical processes

Optical fibers are a natural way to increase the interaction length and to reduce the beam diameter of light fields involved in nonlinear processes [2]. The product $Il_{\text{eff}}$, where $I$ is the light field intensity in an optical fiber and $l_{\text{eff}}$ is the effective interaction length (in a fiber or in the regime of tight focusing), gives the figure of merit [2] for the efficiency of a broad class of nonlinear-optical interactions (including stimulated Raman scattering, as well as self- and cross-phase modulation) and lowering thresholds for a certain class of nonlinear-optical effects (e.g., processes involving stimulated Raman scattering).

The interaction length for tightly focused light beams is confined to the beam waist length. In the case of a Gaussian beam, the beam waist length is approximately equal to $l_{\text{eff}}^{\text{t}} \approx \pi w_0^2/\lambda$, where $w_0$ is the waist radius of the focused beam and $\lambda$ is the radiation wavelength. The maximum waveguide enhancement of a nonlinear-optical process in a fiber with the magnitude of losses $\alpha$ ($\alpha l \gg 1$, $l$ is the fiber length) with respect to the regime of tightly focused pump beams is then given by the well-known expression [2]

$$\frac{I_{\text{f}}\, l_{\text{eff}}^{\text{f}}}{I_{\text{t}}\, l_{\text{eff}}^{\text{t}}} \approx \frac{\lambda}{\pi w_0^2 \alpha}\,, \tag{1}$$

where $I_{\text{f}}$ and $I_{\text{t}}$ are the radiation intensities calculated for the fiber and the regime of tight focusing, respectively.

It is simple to see from Eqn (1) that the waveguide enhancement of nonlinear-optical processes is associated with the possibility of achieving high radiation intensities for a given radiation power due to the light-field confinement to a fiber core with a small radius and large interaction lengths attainable for nonlinear-optical processes in fibers with low radiation losses ($l_{\text{eff}}^{\text{f}} \approx 1/\alpha$). The waveguide enhancement factor and the figure of merit quantifying the lowering of the threshold for nonlinear-optical processes involving stimulated Raman scattering, as can be readily seen from Eqn (1), grow with a decrease in the fiber core diameter.

This recipe for enhancing nonlinear-optical processes remains applicable, however, within a finite range of fiber core diameters. The physical limit is, of course, determined by diffraction effects. As the fiber core diameter becomes smaller and smaller, less and less radiation power remains confined to the fiber core. To quantify the influence of this factor on the waveguide enhancement of nonlinear-optical processes, we represent the product of the intensity of electromagnetic radiation and the effective interaction length in an optical fiber in the following form:

$$I_{\text{f}}\, l_{\text{eff}}^{\text{f}} = \int_0^l \mathrm{d}z\, \frac{P\eta}{\pi a^2} \exp(-\alpha z)\,, \tag{2}$$

where $\eta$ is the ratio of the laser power confined to the fiber core to the total laser power guided by a fiber mode and $a$ is the radius of the fiber core.

Calculating the integral in Eqn (2) and assuming that $\alpha l \gg 1$, as before, we arrive at

$$\xi = \frac{I_{\text{f}}\, l_{\text{eff}}^{\text{f}}}{I_{\text{t}}\, l_{\text{eff}}^{\text{t}}} \approx \frac{\lambda\eta}{\pi a^2 \alpha}\,. \tag{3}$$

Formula (3) allows the distribution of radiation power between the fiber core and the fiber cladding to be included in the waveguide enhancement factor for nonlinear-optical processes in fiber-guided modes. Below, we will employ Eqn (3) to determine the optimal core radius for nonlinear fibers providing the maximum enhancement of nonlinear optical processes and explore the applicability of different asymptotic expressions for estimating the optimal parameters of nonlinear fibers.

### 2.3 The role of diffraction and the physical limit for the waveguide enhancement of nonlinear-optical processes

To calculate the radiation power confined to the fiber core in the $\text{EH}_{1m}$ waveguide mode, we use the following expression, known from the theory of optical fibers [1]:

$$\eta = \frac{\Xi_{\text{core}}}{\Xi_{\text{core}} + \Xi_{\text{clad}}}\,, \tag{4}$$

$$\Xi_{\text{core}} = \frac{kn_{\text{core}}^2}{\beta J_1^2(u)} \Big\{ a_1 a_3 \big[J_0^2(u) + J_1^2(u)\big] + a_2 a_4 \big[J_2^2(u) + J_1(u)\, J_3(u)\big] \Big\}\,, \tag{5}$$

$$\Xi_{\text{clad}} = \frac{kn_{\text{core}}^2}{\beta K_1^2(W)}\, \frac{u^2}{W^2} \Big\{ a_1 a_5 \big[K_0^2(W) - K_1^2(W)\big] + a_2 a_6 \big[K_2^2(W) + K_1(W)\, K_3(W)\big] \Big\}\,. \tag{6}$$

Here,

$$a_1 = \frac{F_2 - 1}{2}\,,\quad a_2 = \frac{F_2 + 1}{2}\,,\quad a_3 = \frac{F_1 - 1}{2}\,,\quad a_4 = \frac{F_1 + 1}{2}\,,$$

$$a_5 = \frac{F_1 - 1 + 2\Delta}{2}\,,\quad a_6 = \frac{F_1 + 1 - 2\Delta}{2}\,,$$

$$F_1 = \frac{(uW)^2}{V^2}\big[b_1 + (1 - 2\Delta)\, b_2\big]\,,\quad F_2 = \frac{V^2}{(uW)^2 (b_1 + b_2)}\,,$$

$$b_1 = \frac{1}{2u}\left(\frac{J_0(u)}{J_1(u)} - \frac{J_2(u)}{J_1(u)}\right),\quad b_2 = -\frac{1}{2W}\left(\frac{K_0(W)}{K_1(W)} + \frac{K_2(W)}{K_1(W)}\right),$$

where $\Delta = (n_{\rm core}^2 - n_{\rm clad}^2)/2n_{\rm core}^2$, $n_{\rm core}$ is the refractive index of the fiber core, $n_{\rm clad}$ is the refractive index of the fiber cladding, $u$ is the eigenvalue of the characteristic equation for the waveguide mode (also known as the mode parameter in the fiber core), $V = ka(n_{\rm core}^2 - n_{\rm clad}^2)^{1/2}$ is the waveguide parameter ($k = 2\pi/\lambda$, $\lambda$ is the radiation wavelength), $\beta = [k^2 n_{\rm core}^2 - (u/a)^2]^{1/2}$ is the propagation constant of the waveguide mode, $W = a(\beta^2 - k^2 n_{\rm clad}^2)^{1/2}$ is the mode parameter in the fiber cladding, $J_n(x)$ are the Bessel functions of the first kind, and $K_n(x)$ are the modified Bessel functions of the second kind.

Solid line *1* in Fig. 3a shows the dependence of the factor $\xi$ on $a$ calculated with the use of Eqns (3)–(6). The maximum values of $\xi$ are achieved with a certain optimal core radius $a_{\rm opt}$. For the factor $\xi$ represented by curve *1* in Fig. 3, $a_{\rm opt} = 0.26$ μm.

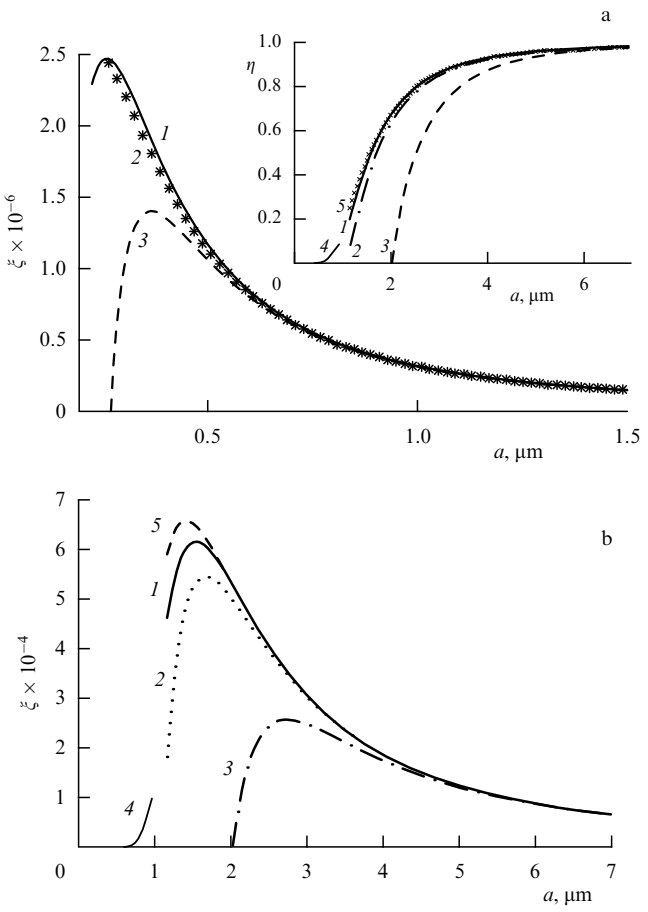


**Figure 3.** The factor $\xi$ of the waveguide enhancement of nonlinear-optical processes as a function of the fiber core radius $a$ (a) for a fiber with the refractive index of the core $n_{\rm core} \approx 1.45$ and the refractive index of the cladding $n_{\rm clad} \approx 1$ ($\Delta \approx 0.26$) and radiation with a wavelength of 1 μm, (b) for radiation with a wavelength of 1 μm in a weakly guiding ($\Delta \approx 5 \times 10^{-3}$) fiber. Calculations were performed with the use of (*1*) Eqns (3)–(6), (*2*) approximate formula (11) with the mode parameter $u$ determined by solving the relevant characteristic equation, (*3*) approximate formula (11) with an assumption of $u \approx 2.4$, (*4*) approximate formula (9) in the regime when $V \ll 1$, and (*5*) approximate formulas (11) and (15). The inset in Fig. 3a shows the fraction $\eta$ of electromagnetic radiation power confined in the core of a weakly guiding ($\Delta \approx 5 \times 10^{-3}$) fiber as a function of the fiber core radius $a$ for radiation with the wavelength 1 μm calculated with the use of (*1*) Eqns (4)–(6), (*2*) approximate formula (10) with the mode parameter $u$ determined by solving the relevant characteristic equation, (*3*) approximate formula (10) with an assumption of $u \approx 2.4$, (*4*) approximate formula (9) with $V \ll 1$, and (*5*) approximate formulas (10) and (15).

To understand the physical factors controlling the behavior of the waveguide enhancement of nonlinear-optical processes as a function of the fiber core radius $a$, we will examine in greater detail the limiting cases of $V \gg 1$ and $V \ll 1$, corresponding to fibers with small and large ratios of the core radius to the radiation wavelength. Physically, these two situations differ by the relation between diffraction and refractive-index-step waveguide confinement effects.

To illustrate this argument, we introduce the characteristic angular beam width $\theta_{\rm d}$, which will serve as a measure of diffraction and which is given, in the case of a Gaussian profile of intensity distribution with the width $w_0$, by the well-known formula [1]

$$\theta_{\rm d} = \arctan \frac{\lambda}{\pi n_{\rm core} w_0} \approx \frac{\lambda}{\pi n_{\rm core} a} . \tag{7}$$

Using Eqn (7), we represent the waveguide parameter $V$ as [1]

$$V = \frac{2\theta_{\rm c}}{\theta_{\rm d}} , \tag{8}$$

where

$$\theta_{\rm c} = \arcsin \left( \frac{1 - n_{\rm clad}^2}{n_{\rm core}^2} \right)^{1/2} \approx \left( \frac{1 - n_{\rm clad}^2}{n_{\rm core}^2} \right)^{1/2}$$

is the critical angle of grazing incidence.

Thus, the waveguide parameter $V$ can be considered as a measure of balance between diffraction and waveguide confinement of a light beam. For fibers with large core radii, having $V \gg 1$, diffraction is negligible and most of the laser power is confined to the fiber core (see the inset in Fig. 3a). In the opposite case of fibers with small core radii, having $V \ll 1$, diffraction becomes significant and a considerable fraction of radiation power is guided in the fiber cladding (the inset in Fig. 3a).

For the fundamental mode of a weakly guiding optical fiber, $\Delta \ll 1$, the fraction $\eta$ of electromagnetic radiation power confined to the fiber core in the limiting case of $V \ll 1$ can be calculated with the use of the following asymptotic expression [1]:

$$\eta \approx 1.261 \, \frac{V^2 + 2}{V^4} \exp \left( -\frac{4}{V^2} \right) . \tag{9}$$

Because of diffraction effects, the factor $\eta$, as can be seen from Eqn (9), rapidly tends to zero as $V \to 0$ (curve *5* in the inset to Fig. 3a).

For large $V$, the fraction of electromagnetic radiation power confined to the fiber core is given by the following asymptotic formula [1]:

$$\eta \approx 1 - \frac{u^2}{V^3} . \tag{10}$$

For $V \geqslant 3$, Eqn (10) is in satisfactory agreement with the results of calculations performed for the ratio $\eta$ with the use of Eqns (4)–(6) (cf. curves *1* and *3* in the inset to Fig. 3a). As the fiber core radius increases, the ratio $\eta$, in accordance with Eqn (10), tends to unity since the role of diffraction becomes negligible as compared with the waveguide confinement of the laser beam due to the refractive-index step.

### 2.4 Asymptotic expressions for the factor of waveguide enhancement of nonlinear-optical processes and numerical simulations

We now use the approximation of Eqn (10) to estimate the waveguide enhancement of nonlinear-optical processes. Substituting Eqn (10) into Eqn (3), we find

$$\xi \approx \frac{\lambda}{\pi a^2 \alpha}\left(1 - \frac{u^2}{V^3}\right). \tag{11}$$

The applicability of the estimate given by Eqn (11) requires additional analysis, since this formula was derived with the use of asymptotic expressions valid for the regime of $V \gg 1$. Such an approach is intrinsically contradictory as the existence of the physical limit for the factor $\xi$ and the optimal value of the fiber core radius is related to diffraction effects, which become negligibly small when $V \gg 1$ [see Eqn (8)].

The waveguide enhancement factor for nonlinear-optical processes calculated with the use of Eqn (11) is shown by curve *2* (asterisks) in Fig. 3a. Comparison of the results of these calculations using approximate relations with the predictions of Eqns (4)–(6) (curve *1* in Fig. 3a) demonstrates that Eqn (11) provides a rather accurate description of the factor $\xi$ for large fiber core radii, i.e., in the case of weak diffraction. The estimate of the optimal fiber core radius obtained with the use of Eqn (11) ($a_{\text{opt}} \approx 0.24$ μm, curve *2* in Fig. 3a) also agrees well with the optimal value of the fiber core radius predicted by Eqns (4)–(6) ($a_{\text{opt}} \approx 0.27$ μm, curve *1* in Fig. 3a).

The use of Eqns (10) and (11) implies the solution of the characteristic equation for the mode parameter $u$ for the relevant waveguide mode. Let us examine now the accuracy of a simplified estimation procedure that uses Eqn (11) with limiting values of the waveguide mode parameter corresponding to large $V$. Setting $u \approx 2.4$ for the fundamental guided mode, differentiating Eqn (11) in $a$, equating the resulting expression to zero, and solving the equation thus obtained, we derive the following simple formula for the optimal value of the fiber core radius, providing the maximum waveguide enhancement of nonlinear-optical processes:

$$a_{\text{opt}} = \left(\frac{5}{2}\varkappa\right)^{1/3}\lambda, \quad \varkappa = \frac{u^2}{(2\pi)^3 (n_{\text{core}}^2 - n_{\text{clad}}^2)^{3/2}}. \tag{12}$$

Setting $n_{\text{core}} \approx 1.45$ and $n_{\text{clad}} \approx 1$, we arrive at the following estimate for the optimal fiber core radius: $a_{\text{opt}} \approx 0.37\lambda$. In view of the approximation $u \approx 2.4$, the accuracy of Eqn (12) is lower than the accuracy of Eqns (10) and (11). Curve *3* in Fig. 3a shows the dependence of the factor $\xi$ on the fiber core radius calculated with the use of Eqn (11) in the approximation of $u \approx 2.4$ for radiation with a wavelength of 1 μm and the above-specified refractive indices of the core and the cladding.

Expression (12) can provide only order-of-magnitude estimates of the optimal fiber core radius and the maximum enhancement factor for nonlinear-optical processes (curve *3* in Fig. 3a). This approximation systematically overestimates the factor $\xi$ since it employs Eqn (11) where the $V$-dependent mode parameter $u$ is replaced by its upper-bound value. The maximum value of the factor $\xi$ in the dependence represented by curve *3* in Fig. 3a is achieved with the core radius meeting Eqn (12), $a_{\text{opt}} \approx 0.37$ μm. Being correct in its order of magnitude, this estimate still differs noticeably in its value from the result obtained with the use of Eqns (3)–(6).

The main advantages of the estimate given by Eqn (12) are associated with its simplicity and the insights it gives into the influence of fiber parameters on the optimal core radius and the maximum value of the factor $\xi$. The waveguide enhancement factor in this approximation is given by

$$\xi = \frac{4\pi}{\alpha\lambda}\,(n_{\text{core}}^2 - n_{\text{clad}}^2)\,\psi(V), \tag{13}$$

where

$$\psi(V) = \frac{1}{V^2}\left(1 - \frac{u^2}{V^3}\right). \tag{14}$$

When the mode parameter $u$ is estimated by its upper-bound value ($u \approx 2.4$ for the fundamental mode), the function $\psi(V)$ depends only on the type of the waveguide mode and reaches its maximum value with $V_{\text{opt}} = (5/2)^{1/3}u^{2/3}$. Expression (13) shows, in particular, that a decrease in the optimal core radius and, consequently, the increase [in view of Eqn (3)] in the maximum waveguide enhancement of nonlinear-optical processes can be achieved by increasing the refractive-index step (parameter $\Delta$) between the core and the cladding of the fiber.

Figure 3b displays the dependences of the factor $\xi$ on the fiber core radius $a$ for weakly guiding fibers with $\Delta \approx 5 \times 10^{-3}$. The maximum value of the factor $\xi$ for 1-μm radiation is achieved in this case with a core radius equal to 1.5 μm (curve *1* in Fig. 3b). The factor $\xi$ under these conditions is nearly 40 times less than in the case of a fiber with a limiting refractive-index step for fused silica structures ($\Delta \approx 0.26$, Fig. 3a).

In the case of weakly guiding fibers, approximate formula (11) also provides a sufficiently accurate estimate of the optimal fiber core radius and the maximum value of the factor $\xi$ (curve *2* in Fig. 3b). Finally, Eqn (11), where the mode parameter $u$ is replaced by its upper-bound value ($u \approx 2.4$), can provide only order-of-magnitude estimates for these parameters (curve *3* in Fig. 3b). This latter approximation, however, gives a qualitatively correct prediction for a decrease in the maximum value of the factor $\xi$ with a lowering of the refractive-index step.

The difference of the refractive indices squared, $n_{\text{core}}^2 - n_{\text{clad}}^2$, appearing in Eqn (13), is approximately 50 times higher in the case of the dependences presented in Fig. 3a than the parameter $n_{\text{core}}^2 - n_{\text{clad}}^2$ for the dependences of Fig. 3b. The corresponding ratio of the values of the factor $\xi$, calculated with the use of the exact formulas (3)–(6), is approximately 40 (cf. curves *1* in Figs 3a and 3b). In practice, the highest values of the parameter $\Delta$ can be achieved with tapered fibers [51, 52] and microstructure fibers with high air-filling fractions [15, 60]. The fibers of these types, therefore, open the way to attack the physical limit of the waveguide enhancement of nonlinear-optical interactions.

The analysis performed above shows that the approximation where the mode parameter in Eqns (11), (13), and (14) is replaced by its upper-bound value does not always provide a high accuracy of estimates of the factors $\eta$ and $\xi$. The accuracy of Eqns (13) and (14) can sometimes be improved by using the following asymptotic representation for the parameter $u$ of the fundamental waveguide mode [1]:

$$u \approx 2.405 \exp\left(-\frac{1+\Delta}{V}\right). \tag{15}$$

Formulas (13) and (14), in combination with the asymptotic representation of Eqn (15), provide a satisfactory accuracy in calculations of the power guided in the fiber core (curve *5* in the inset in Fig. 3a) and the waveguide enhancement factor $\xi$ (curve *5* in Fig. 3b), allowing the optimal values of the fiber core radius and the maximum values of the factor $\xi$ to be calculated with reasonable accuracy. The error in the estimation of the factor $\eta$ based on Eqns (10) and (15) in the intermediate range of $V$ corresponding to the maximum values of the waveguide enhancement increases with the growth of the parameter $\Delta$. The accuracy of estimates on the optimal value of the fiber core radius and the maximum value of the factor $\xi$ lowers under these conditions.

### 2.5 Stimulated Raman and coherent anti-Stokes Raman scattering in guided modes of hollow photonic-crystal fibers

In this section we will discuss the generic idea of enhancing SRS- and CARS-type nonlinear-optical processes with the use of hollow-core microstructure and photonic-crystal fibers. Hollow fibers are currently widely employed [61] for the generation of ultrashort pulses using Kerr-nonlinearity-induced self- and cross-phase modulation [62 – 64] and stimulated Raman scattering [65], as well as for high-order harmonic generation [66 – 69] and improving the sensitivity of gas-phase analysis based on four-wave mixing spectroscopy [70 – 72].

In hollow fibers, the refractive index of the core, $n_{\rm core}$, is lower than the refractive index of the cladding $n_{\rm clad} = \sqrt{\varepsilon_{\rm clad}}$. Therefore, the propagation constants of guided modes in hollow fibers,

$$\beta = \left[k_{\rm core}^2 - \left(\frac{u_n}{a}\right)^2\right]^{1/2} = \left[k_{\rm clad}^2 - \left(\frac{W_n}{a}\right)^2\right]^{1/2},$$

have nonzero imaginary parts. The propagation of light in such fibers is accompanied by radiation losses. Here, $k_{\rm core} = n_{\rm core}\omega/c$, $k_{\rm clad} = n_{\rm clad}\omega/c$, $u_n$ is the eigenvalue of the characteristic equation for the waveguide mode with the set of mode indices $n$, and $W_n$ is the transverse wave number of the fiber cladding mode.

For $EH_{mn}$ modes of a hollow fiber with the inner radius $a$ and the refractive index of the gas filling the fiber core $n_{\rm core} \approx 1$, the radiation intensity attenuation coefficient is given by [73, 74]

$$\alpha = \left(\frac{u_{mn}}{2\pi}\right)^2 \frac{\lambda^2}{a^3} \frac{n^2+1}{(n^2-1)^{1/2}}, \qquad (16)$$

where $n = n_{\rm clad}$. Such behavior of the magnitude of optical losses prevents one from using hollow fibers with very small inner diameters in nonlinear-optical experiments. Using Eqn (16), we find that the magnitude of radiation losses for the fundamental mode of a hollow fiber with a fused silica cladding and an inner radius of 7 μm may exceed 6.5 $\rm cm^{-1}$ for 1-μm radiation, which imposes serious limitations on applications of such fibers.

To qualitatively illustrate the idea of reducing the optical losses in a hollow fiber with a periodic microstructure cladding relative to the optical losses in a hollow fiber with a solid cladding, we will employ the result well known from the analysis of radiation propagation in a planar waveguide with a periodic cladding [75]. The decrease in the magnitude of optical losses in a hollow planar waveguide with a periodic cladding relative to the magnitude of optical losses in a hollow planar waveguide with a solid cladding can be quantified by determining the ratio of the logarithm of the coefficient of reflection from the periodic structure to the logarithm of the coefficient of reflection from the walls of a hollow waveguide.

Around the center of the photonic band gap in the reflection spectrum of the periodic structure in a waveguide cladding with a sufficiently large number of layers $N$, the coefficient of optical losses $\alpha_{\rm PBG}$ in a hollow planar waveguide with a periodic cladding decreases exponentially relative to the coefficient of losses $\alpha_{\rm h}$ in a hollow waveguide with a solid cladding, with the increase in the number of modulation periods of the refractive index in the waveguide cladding,

$$\frac{\alpha_{\rm PBG}}{\alpha_{\rm h}} \propto a \exp\left(-2|\varkappa|Nd\right),$$

where $\varkappa$ is the coupling coefficient of the forward and backward waves in the periodic structure of the waveguide cladding and $d$ is the modulation period of the refractive index in the waveguide cladding. Thus, hollow waveguides with periodic cladding allow the optical losses characteristic of hollow-waveguide modes to be considerably reduced.

Hollow-core photonic-crystal fibers seem to be ideally suited for highly efficient waveguide SRS and CARS interactions. Transmission spectra of hollow photonic-crystal fibers may display isolated peaks [38 – 40], which can be employed to radically enhance nonlinear-optical interactions of spectrally isolated optical signals. Stimulated Raman scattering and coherent anti-Stokes Raman scattering belong to this class of nonlinear-optical processes. In the following sections, we will consider the ways to optimize parameters of hollow photonic-crystal fibers for a maximum enhancement of SRS and CARS processes.

### 2.6 Stimulated Raman scattering

**2.6.1 The influence of waveguide losses and the optimal fiber length.** To assess the influence of waveguide losses on stimulated Raman scattering in a hollow-core fiber with a solid or photonic-crystal cladding having a length $l$, we employ the solution to the stationary SRS equation for the intensity of the Stokes signal, ignoring pump-depletion effects [2]:

$$I_{\rm s}(l) = I_{\rm s}(0) \exp\left(gI_0 l_{\rm eff} - \alpha_{\rm s} l\right), \qquad (17)$$

where $g$ is the SRS gain; $I_0$ is the initial intensity of the pump;

$$l_{\rm eff} = \frac{1}{\alpha_{\rm p}}\left[1 - \exp\left(-\alpha_{\rm p} l\right)\right] \qquad (18)$$

is the effective interaction length; and $\alpha_{\rm p}$ and $\alpha_{\rm s}$ are the coefficients of losses at the pump and Stokes frequencies, respectively.

The intensity of the SRS signal, as can be seen from Eqns (17) and (18), is determined by the SRS gain, the intensity of pump radiation, and the coefficients of losses at the frequencies of pump and Stokes radiation. Hollow-core microstructure fibers with core diameters on the order of 13 – 15 μm [38, 40] allow pump radiation intensities on the order of $5 \times 10^{10} - 5 \times 10^{12}$ W $\rm cm^{-2}$ to be achieved with 100-fs pulses having an energy of 0.01 – 1 μJ. Figure 4 displays the Stokes signal intensity as a function of the fiber length and the coefficients of losses at the frequencies of pump (Fig. 4a) and

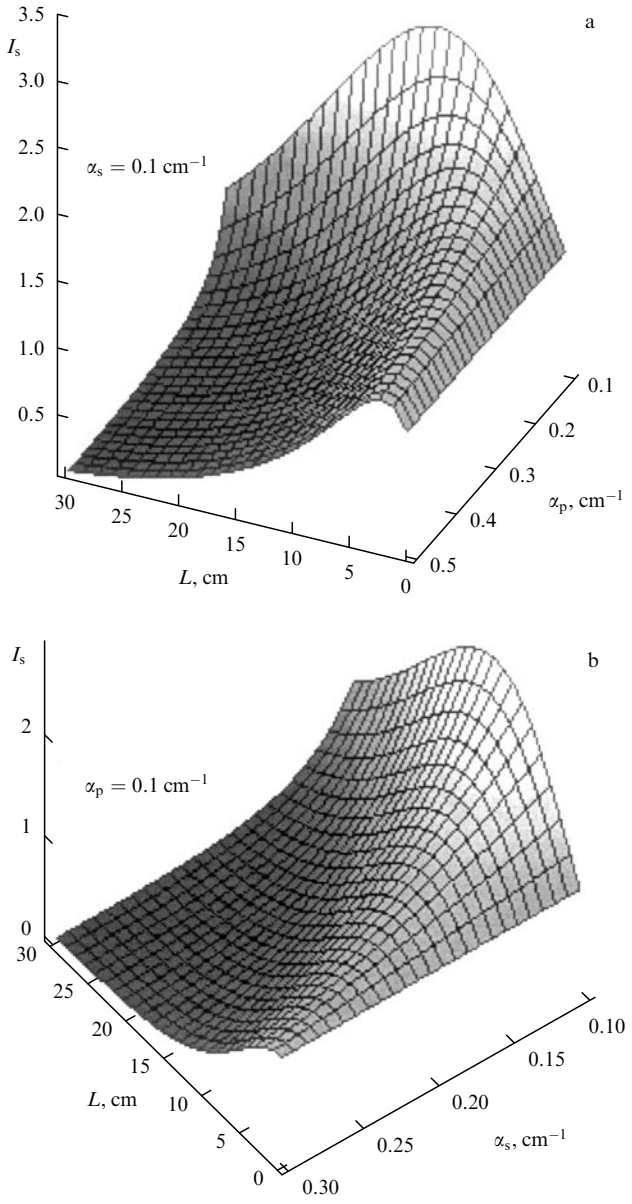


**Figure 4.** The intensity of the SRS signal as a function of the fiber length $L$ and the attenuation coefficients of (a) the pump and (b) the Stokes signal for $gI_0 = 0.3$ cm$^{-1}$.

Stokes (Fig. 4b) radiation calculated for the magnitudes of losses characteristic of photonic-crystal fibers with a core diameter of 13–15 μm, with the assumption that $gI_0 = 0.3$ cm$^{-1}$. Such values of the $gI_0$ factor can be achieved in the case of hollow-core fibers filled with molecular hydrogen ($b^2 = \left[(1/3)\,\mathrm{Sp}(\partial\alpha_{ij}/\partial Q)\right]^2 \approx 4 \times 10^{-34}$ cm$^4$, where $\partial\alpha_{ij}/\partial Q$ is the derivative of the electronic polarizability of molecules in the generalized coordinate $Q$ defining the nuclear configuration) or nitrogen ($b \approx 1.6 \times 10^{-33}$ cm$^4$) at atmospheric pressure with the above-specified levels of laser radiation intensity.

As can be seen from Eqns (17) and (18), the Stokes signal grows only when $gI_0 > \alpha_s$. Otherwise, waveguide losses result in an exponential decay of the Stokes signal. For a small $l$, such that $\alpha_p l$, $\alpha_s l$, $gI_0 l \ll 1$, the Stokes signal grows linearly as a function of $l$ (Fig. 4). For lengths $l$ substantially exceeding the attenuation length of pump radiation, $\alpha_p l \gg 1$, waveguide losses lead to a noticeable attenuation of pump radiation. The intensity of the Stokes signal exponentially decreases under these conditions with the growth in $l$ with a characteristic spatial scale defined by the attenuation length of the Stokes signal.

Thus, stimulated Raman scattering in a fiber with losses can be optimized with some fiber length $l_{\mathrm{opt}}^{\mathrm{SRS}}$, providing the maximum efficiency for the generation of the Stokes component (Fig. 4). Using Eqns (17) and (18), we derive the following expression for the optimal fiber length $l_{\mathrm{opt}}^{\mathrm{SRS}}$ (with $gI_0 > \alpha_s$):

$$l_{\mathrm{opt}}^{\mathrm{SRS}} = \frac{1}{\alpha_p} \ln \frac{gI_0}{\alpha_s} . \tag{19}$$

Substituting this expression for the optimal fiber length into Eqn (17), we find that the maximum integral SRS gain in a hollow fiber is given by

$$G = \frac{gI_0}{\alpha_p} - \frac{\alpha_s}{\alpha_p}\left(1 + \ln \frac{gI_0}{\alpha_s}\right) . \tag{20}$$

In the case of $gI_0 \gg \alpha_s, \alpha_p$, the second term in Eqn (20) is small as compared with the first term. The maximum increase in the integral SRS gain in a hollow fiber relative to the regime of tight focusing is then equal to

$$\zeta = \frac{\lambda}{\pi a^2 \alpha_p} . \tag{21}$$

Comparing Eqns (3) and (21), we find that the upper bound of the increase in the integral SRS gain predicted by Eqns (17)–(20) for stationary SRS coincides with the estimate of the waveguide enhancement factor of nonlinear-optical processes given by Eqn (3), which was derived from general physical considerations. As can be seen from Eqn (21), even short hollow photonic-crystal and microstructure fibers can provide a substantial SRS enhancement (see Fig. 4). A radical lowering of the SRS threshold in hollow microstructure fibers was observed earlier by Benabid et al. [41]. We will show in Section 2.7 that such fibers may allow an even more substantial enhancement of nonlinear signal generation in the case of coherent anti-Stokes Raman scattering [42].

**2.6.2. Group-delay and group-velocity-dispersion effects.** Group-delay effects limit the length of nonlinear-optical interaction, giving rise to a walk-off of the pump and Stokes pulses within the characteristic length

$$l_w = \frac{\tau}{\left|v_p^{-1} - v_s^{-1}\right|},$$

where $v_p$ and $v_s$ are the group velocities of the pump and Stokes pulses, respectively, and $\tau$ is the pump pulse duration. Group-velocity dispersion leads to the spreading of light pulses within the characteristic length

$$l_d = \frac{\tau^2}{|\beta_2|} .$$

In view of these factors, the effective length of pump–Stokes pulse interaction should be re-defined as

$$L_{\mathrm{eff}} = \min\left(l_{\mathrm{eff}}, l_w, l_d\right) .$$

The influence of the group-velocity mismatch and group-velocity dispersion can be reduced, with an appropriate choice of fiber and gas parameters, by using the dispersion of waveguide modes [76]. Physically, this opportunity can be understood by comparing the group velocity of a light pulse propagating in a gas-filled hollow fiber (the solid line in Fig. 5a),

$$v^{pq} = \left(\frac{\partial K^{pq}}{\partial \omega}\right)^{-1}, \tag{22}$$

with the group velocity of a light pulse in the same gas, but in the absence of a waveguide (the dashed line in Fig. 5a),

$$v = \left(\frac{\partial k}{\partial \omega}\right)^{-1} = \frac{c}{n}\left(1 + \frac{\omega}{n}\,\frac{\partial n}{\partial \omega}\right)^{-1}. \tag{23}$$

Here, $K^{pq}$ is the propagation constant corresponding to the relevant waveguide mode of a hollow fiber with mode indices $p$ and $q$, $k = n\omega/c$, and $n$ is the refractive index of the gas. The propagation constant of a light pulse in a gas-filled hollow fiber is related to the free-space wave number $k$ of this pulse in the same gas by the expression

$$K^{pq} = \left(k^2 - h_{pq}^2\right)^{1/2},$$

where the quantity $h_{pq}$ can be found from the characteristic equation for the waveguide mode of the hollow fiber.

In particular, using the well-known formulas for the propagation constants of guided modes in hollow fibers [73], we arrive at the following expression for the group velocity of a light pulse with a transverse field distribution corresponding to the $EH_{1m}$ mode of a hollow fiber:

$$v_m = v_0\left[1 - \frac{1}{2}\left(\frac{u_m c}{a\omega n}\right)^2\right], \tag{24}$$

where

$$v_0 = \frac{c}{n}\left(1 + \frac{\omega}{n}\,\frac{\partial n}{\partial \omega}\bigg|_{\omega_l}\right)^{-1}$$

is the group velocity of the light pulse in the gas in the absence of a hollow fiber.

The group-velocity mismatch in a gas-filled hollow fiber can be then represented as a sum of two terms,

$$\Delta K_m = \Delta K_0 + \Delta K_m^{\mathrm{w}}, \tag{25}$$

where $\Delta K_0$ and $\Delta K_m^{\mathrm{w}}$ are the components of the group-velocity mismatch due to the gas and waveguide dispersion, respectively.

The waveguide component of the group-velocity mismatch, as follows from Eqn (24), is inversely proportional to the square of the inner radius of a hollow fiber, scaling as

$$\Delta K_m^{\mathrm{w}} \propto a^{-2}.$$

Physically, this circumstance implies that larger group-velocity mismatches can be compensated in hollow fibers with smaller inner diameters. The dashed lines in Figs 5a and 5b represent the group index and the group-velocity dispersion of molecular hydrogen at a pressure of 0.5 atm as functions of the wavelength. The dotted lines in the same figures show the wavelength dependences of the group index and the group-velocity dispersion for the $EH_{11}$ mode of a hollow fiber with an inner radius of 68 μm. The resulting wavelength dependences of the group index and the group-velocity dispersion, including the waveguide dispersion component, are shown by the solid lines.

With an appropriate choice of hollow-fiber parameters, as can be seen from the dependences presented in Figs 5a and 5b, the waveguide dispersion can reduce the group delay and the group-velocity dispersion for the pump and Stokes pulses. At a certain wavelength (560 nm in Fig. 5b), the waveguide component of group-velocity dispersion exactly compensates for the material group-velocity dispersion, giving rise to a point of zero group-velocity dispersion, which is missing from the dispersion profile of the gas (the dashed line in Fig. 5b). The wavelength of zero group-velocity dispersion can be found by a double differentiation of the expression for the propagation constant of guided modes. This procedure yields the following approximate formula:

$$k_2 = v_0^{-2}\left(\frac{\lambda}{2\pi n}\right)^3\left(\frac{u_m}{a}\right)^2, \tag{26}$$

where $k_2$ is the material component of group-velocity dispersion.

As can be seen from Eqn (26), the wavelength of zero group-velocity dispersion can be tuned by changing the inner radius of the fiber and the type of waveguide mode, as well as by varying the pressure and the sort of gas filling the fiber core. The waveguide component of group-velocity dispersion scales as $\lambda^3/a^2$ when the radiation wavelength and the inner fiber radius are varied.

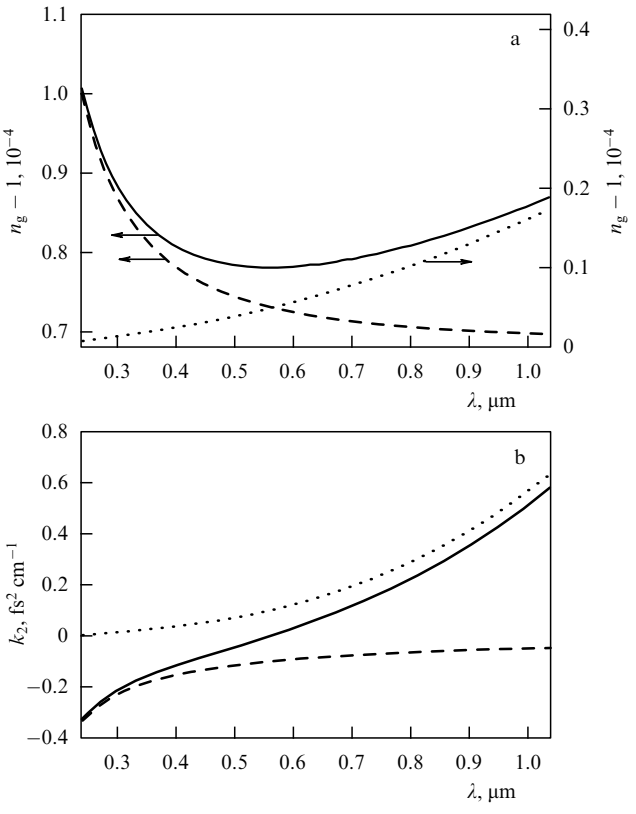


**Figure 5.** (a) The group index $n_g = c/v_g$ and (b) group-velocity dispersion calculated as functions of the wavelength (dashed lines) for molecular hydrogen, (dotted lines) the $EH_{11}$ waveguide mode, and (solid lines) the $EH_{11}$ mode of a hollow fiber filled with molecular hydrogen. The gas pressure is 0.5 atm. The inner radius of the fiber is 68 μm.

### 2.7 Coherent anti-Stokes Raman scattering

Coherent anti-Stokes Raman scattering [77–82] is one of the most convenient, efficient, and practical methods of nonlinear coherent spectroscopy. Waveguide regimes substantially improve the sensitivity and extend the applicability range of CARS spectroscopy [70, 83–87]. The enhancement of CARS in gas-filled hollow fibers was experimentally demonstrated back in the 1970s [70]. These experiments have opened the nonlinear-optical chapter in the history of hollow waveguides.

Similarly to SRS, CARS is enhanced in hollow fibers due to the confinement of electromagnetic radiation to a small-size fiber core and large interaction lengths. We will show below that the waveguide enhancement in the case of CARS in hollow microstructure fibers with a small inner radius may exceed an analogous enhancement attainable for the SRS process. We will demonstrate that the waveguide enhancement of CARS in a hollow microstructure fiber relative to the regime of tight focusing scales as $\lambda^2/\alpha^2 a^4$, allowing substantial enhancement factors to be achieved with hollow-core microstructure fibers having small inner diameters.

We start with the expression for the power of the CARS signal generated through the three-color process $\omega_s = \omega_0 + \omega_1 - \omega_2$ [88]:

$$P_{\mathrm{CARS}} = 1.755 \times 10^{-5}\, \frac{\omega_s^4 k_0 k_1 k_2}{c^4 k_s^2 k'}\, D^2 \left|\chi_{\mathrm{eff}}^{(3)}\right|^2 P_0 P_1 P_2 F_2 \,. \quad (27)$$

Here, $k_0$, $k_1$, $k_2$, and $k_s$ are the wave numbers of light fields (propagation constants of waveguide modes) with frequencies $\omega_0$, $\omega_1$, $\omega_2$, and $\omega_s$, respectively; $P_0$, $P_1$, and $P_2$ are the powers of the fields with frequencies $\omega_0$, $\omega_1$, and $\omega_2$, respectively; $\chi_{\mathrm{eff}}^{(3)}$ is the effective combination of cubic nonlinear-optical susceptibility tensor components corresponding to the chosen set of polarization vectors of pump and signal fields; $D$ is the frequency degeneracy factor of the four-wave mixing process defined after Maker and Terhune [89]; and

$$F_2 = \frac{2k'}{\pi b} \int_0^\infty \mathrm{d}R\, 2\pi R \times \left| \int_{-\zeta}^{\xi} \mathrm{d}\xi'\, \frac{\exp\left[(\mathrm{i}/2)\, b\Delta k \xi'\right]}{(1+\mathrm{i}\xi')(k'' - \mathrm{i}k'\xi')H} \exp\left(-\frac{R^2}{bH}\right) \right|^2 \quad (28)$$

is the phase-matching integral, where $\Delta k = k_s - (k_0 + k_1 - k_2)$, $k' = k_0 + k_1 - k_2$, $k'' = k_0 + k_1 + k_2$, $\xi = 2(z-f)/b$, $\zeta = 2f/b$, $b = n_j \omega_j w_0^2/c$ is the confocal parameter, $w_0$ is the beam waist radius, and

$$H = \frac{(1+\xi')^2}{k'' - \mathrm{i}k'\xi'} - \mathrm{i}\,\frac{\xi' - \xi}{k'} \,. \quad (29)$$

In the limiting case of tight focusing, when the confocal parameter $b$ is much less than the length of the nonlinear medium $l$, $b \ll l$, no increase in the CARS power can be achieved by reducing the pump beam waist radius because of the simultaneous decrease in the interaction length. Mathematically, this well-known result is a consequence of the tight-focusing limit existing for the phase-matching integral [88]:

$$F_2 = 4\pi^2\, \frac{\exp\left[-(k''/k')|\Delta k|\, b\right]}{(1 + k''/k')^2} \,. \quad (30)$$

In the case of small phase mismatch, $\Delta k l \ll \pi$, this limit is written as

$$F_2 = \frac{4\pi^2}{(1 + k''/k')^2} \,. \quad (31)$$

In the opposite limiting case of loosely focused pump beams, $b \gg l$, the phase-matching integral in the regime of weak absorption is reduced to [88]

$$F_2 = \frac{k'}{k''}\, \frac{4l^2}{b^2}\, \frac{\sin^2(\Delta k l/2)}{(\Delta k l/2)^2} \,. \quad (32)$$

In the case of small phase mismatch, Eqn (32) gives

$$F_2 = \frac{k'}{k''}\, \frac{4l^2}{b^2} \,. \quad (33)$$

Assuming that the beam waist radius of focused pump beams is matched with the inner radius $a$ of the hollow fiber having length $l$, we find from Eqns (32) and (33) that the waveguide CARS enhancement factor scales as $\lambda^2 l^2/a^4$ (see also [70, 71, 88]). The mode-overlapping integral should be generally included to describe the influence of transverse field profiles in the waveguide modes involved in the CARS process [83]. The fundamental limitation of waveguide CARS in hollow fibers, experimentally demonstrated in [70–72], comes from optical losses, whose magnitude scales as $\lambda^2/a^3$ with a decrease in the fiber inner radius $a$ in the case of conventional, solid-cladding hollow fibers [62].

The influence of optical losses and phase-mismatch effects on the CARS process in the loose-focusing regime can be included through the factor [78]

$$M \propto \exp\left[-(\Delta\alpha + \alpha_4)\, l\right] \frac{\sinh^2(\Delta\alpha l/2) + \sin^2(\Delta k l/2)}{(\Delta\alpha l/2)^2 + (\Delta k l/2)^2}\; l^2 \,, \quad (34)$$

where $\Delta\alpha = (\alpha_1 + \alpha_2 + \alpha_3 - \alpha_4)/2$; $\alpha_1$, $\alpha_2$, $\alpha_3$, and $\alpha_4$ are the magnitudes of optical losses at the frequencies $\omega_0$, $\omega_1$, $\omega_2$, and $\omega_s$, respectively.

It is straightforward to see from Eqn (34) that the amplitude of the CARS signal in a lossy waveguide reaches its maximum at some optimal length $l_{\mathrm{opt}}^{\mathrm{CARS}}$ (Fig. 6), which is given by

$$l_{\mathrm{opt}}^{\mathrm{CARS}} = \frac{1}{\Delta\alpha} \ln \frac{\alpha_1 + \alpha_2 + \alpha_3}{\alpha_4} \,. \quad (35)$$

With $\alpha_1 \approx \alpha_2 \approx \alpha_3 \approx \alpha_4 = \alpha$, Eqn (35) yields

$$l_{\mathrm{opt}}^{\mathrm{CARS}} = \frac{\ln 3}{\alpha} \,. \quad (36)$$

Then, setting $w_0 = 0.73a$ for the best matching of input beams with the fiber mode radius [73], we substitute Eqn (36) for the optimal interaction length into Eqns (33) and (34) to arrive at the following expression for the waveguide CARS enhancement factor in the regime of phase matching:

$$\mu = 1.3 \times 10^{-3}\, \frac{(k' + k'')^2}{k'k''}\, \frac{\lambda^2}{\alpha^2 a^4} \,. \quad (37)$$

Here, we assume that the refractive index of the gas filling the fiber core is approximately equal to unity and take into

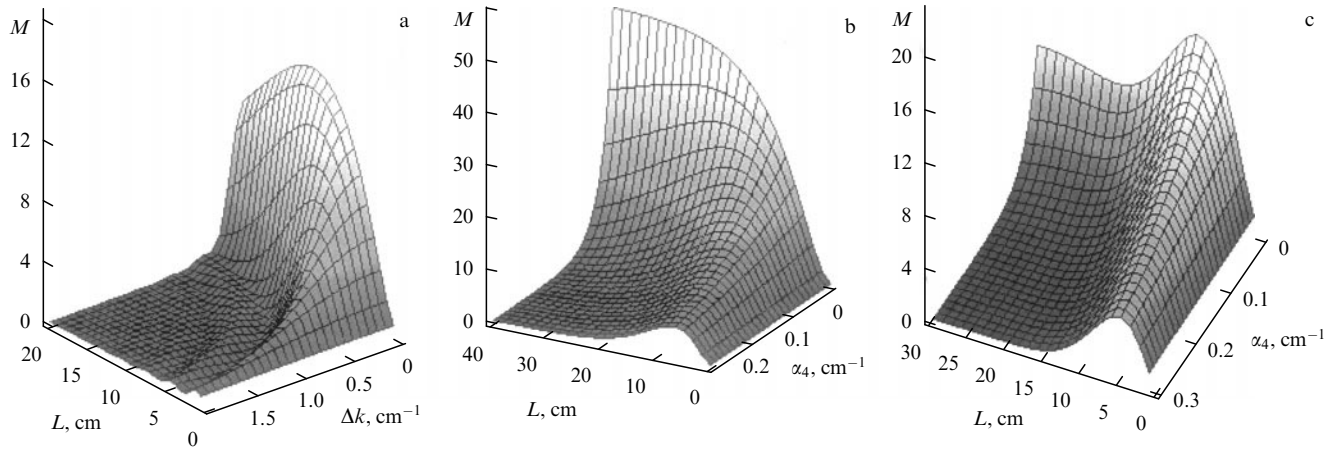


**Figure 6.** The factor $M$, describing the influence of propagation effects on waveguide coherent anti-Stokes Raman scattering, as a function of the fiber length $L$, the phase mismatch, and attenuation coefficient $\alpha_4$ for (a) $\alpha_1 = \alpha_2 = \alpha_3 = \alpha_4 = 0.1$ cm$^{-1}$; (b) $\alpha_1 = \alpha_2 = \alpha_3 = 0.1$ cm$^{-1}$ and $\Delta\beta = 0$; (c) $\alpha_1 = \alpha_2 = \alpha_3 = 0.1$ cm$^{-1}$ and $\Delta\beta = 0.3$ cm$^{-1}$.

consideration that for $\Delta k = 0$ and $l = l_{\rm opt}^{\rm CARS} = \ln 3/\alpha$,

$$M = \frac{(\sqrt{3} - 1/\sqrt{3})^2}{(3\ln 3)^2} \approx 0.123\,.$$

Plugging optical losses of a solid-cladding hollow fiber into the CARS enhancement factor by substituting Eqn (16) into Eqn (37) with $u_n = 2.4$ for the limiting eigenvalue of the $EH_{11}$ mode, we derive the following expression for the factor of CARS enhancement in a solid-cladding hollow fiber relative to the tight-focusing regime in the case of exact phase matching, $\Delta k = 0$:

$$\rho = 6.1 \times 10^{-2}\ \frac{(k' + k'')^2}{k'k''} \left(\frac{a}{\lambda}\right)^2 \frac{n^2 - 1}{(n^2 + 1)^2}\,. \qquad (38)$$

The dependence of the CARS enhancement factor $\rho$ in a solid-cladding hollow fiber on the inner fiber radius $a$ is shown by curve *1* in Fig. 7a. Optical losses, growing with a decrease in the inner radius of the hollow fiber, limit CARS enhancement in hollow fibers of this type.

The situation radically changes in the case of a hollow microstructure fiber. The waveguide enhancement of the CARS process in such fibers relative to the tight-focusing regime is given by Eqn (37). Waveguide losses in this case are still the main physical factors limiting the waveguide CARS enhancement (Fig. 6). However, the magnitude of optical losses in hollow microstructure fibers may be sufficiently low even for fibers with small inner diameters. The magnitude of optical losses for such fibers, as shown in [41], may be on the order of 1–3 dB m$^{-1}$ in the case of fibers with hollow core diameters of about 15 μm. Curves *2* and *3* in Fig. 7a show the CARS enhancement factor $\mu$ calculated as a function of the inner radius of a hollow microstructure fiber for two magnitudes of optical losses, $\alpha = 0.1$ and 0.01 cm$^{-1}$.

In the case of small inner radii, hollow microstructure fibers, as can be readily seen from Eqns (37) and (38) for the parameters $\rho$ and $\mu$, provide much higher CARS enhancement factors than solid-core hollow fibers. According to Fig. 2a, the CARS enhancement factor in hollow microstructure fibers with the magnitude of optical losses equal to 0.1 and 0.01 cm$^{-1}$ exceeds the CARS enhancement factor in

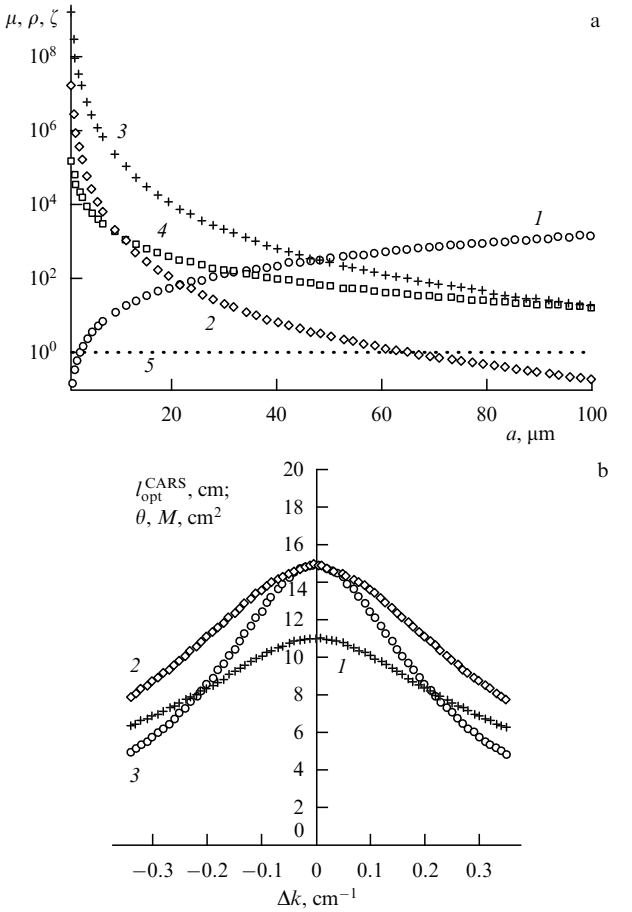


**Figure 7.** (a) Figures of merit $\rho$ and $\mu$ for the efficiency of waveguide CARS in (*1*) a standard hollow fiber with a solid cladding and (*2*, *3*) a hollow microstructure fiber with the attenuation coefficient $\alpha = 0.1$ (*2*) and 0.01 cm$^{-1}$ (*3*) as functions of the inner radius $a$ of the fiber. Curve *4* shows the figure of merit $\xi$ for SRS efficiency in a hollow microstructure fiber with the attenuation coefficient $\alpha = 0.01$ cm$^{-1}$ as a function of the inner radius $a$ of the fiber. Dotted line *5* represents the efficiency of CARS in the regime of tight focusing. The radiation wavelength is 0.5 μm. (b) The optimal length $l_{\rm opt}^{\rm CARS}$ for the CARS process (curve *1*), parameter $\theta = 0.123(l_{\rm opt}^{\rm CARS})^2$ (curve *2*), and the factor $M$ (curve *3*) calculated as functions of the phase mismatch $\Delta k$ by numerically solving Eqn (39) with $\alpha_1 = \alpha_2 = \alpha_3 = \alpha_4 = 0.1$ cm$^{-1}$.

solid-cladding hollow fibers for core radii less than 20 and 45 μm, respectively.

For hollow fibers with small core radii, the waveguide enhancement factor for the CARS process provided by microstructure fibers may be several orders of magnitude higher than the waveguide enhancement factor attainable with solid-cladding fibers (Fig. 7a). We assume in this consideration that the core–cladding geometry in a hollow microstructure fiber supports at least one air-guided mode even for small values of the inner radius of the fiber. A qualitative analysis of the number of air-guided modes supported by hollow photonic-crystal fibers has been provided by Cregan et al. [38]. More detailed numerical simulations of air-guided modes in such fibers have been performed by Broeng et al. [90].

Comparison of Eqns (21) and (37) shows that the scaling law of the waveguide CARS enhancement factor as a function of the magnitude of optical losses, fiber inner radius, and radiation wavelength differs from the corresponding scaling law of the waveguide SRS enhancement factor. Physically, this difference stems from differences in scattering mechanisms involved in SRS and CARS, with SRS and CARS signals building up in different fashions as functions of the interaction length and pump field amplitudes [cf. Eqns (17) and (27)]. The difference in waveguide enhancement factors for SRS and CARS suggests different strategies for optimizing fibers designed to enhance these processes. Due to the stronger dependence of the CARS efficiency on the inner radius of a hollow fiber, the limiting waveguide enhancement for CARS in hollow microstructure fibers may noticeably exceed similar factors for SRS (cf. curves *2–4* in Fig. 7a).

In the case of nonzero phase mismatch, the optimal length for the CARS process can be found from the transcendental equation that immediately follows from Eqn (34),

$$\Delta\alpha \sinh\left(\Delta\alpha l_{\mathrm{opt}}^{\mathrm{CARS}}\right) + \Delta k \sin\left(\Delta k l_{\mathrm{opt}}^{\mathrm{CARS}}\right) + (\Delta\alpha + \alpha_4)\left[\cos\left(\Delta k l_{\mathrm{opt}}^{\mathrm{CARS}}\right) - \cosh\left(\Delta\alpha l_{\mathrm{opt}}^{\mathrm{CARS}}\right)\right] = 0 . \quad (39)$$

Curve *1* in Fig. 7b shows the optimal length calculated by numerically solving Eqn (39) as a function of the phase mismatch $\Delta k$. The growth in the phase mismatch $\Delta k$, as can be seen from this dependence, reduces the optimal fiber length for the CARS process. Curves *2* and *3* of the same figure represent the parameter $0.123\,(l_{\mathrm{opt}}^{\mathrm{CARS}})^2$, corresponding to the approximation of Eqn (37), and the factor $M$ calculated by numerically solving Eqn (39).

Comparison of curves *1–3* in Fig. 7b visualizes the deviation of the factor $M$, which includes the influence of waveguide losses and the phase mismatch, from the approximate dependence given by Eqn (37), which was employed in our analysis to find the limiting waveguide enhancement factors for the CARS process in hollow fibers. The results presented in Fig. 7b show that the approximation of Eqn (37) works well in the case of perfect phase matching, when the factor $M$ coincides with $0.123\,(l_{\mathrm{opt}}^{\mathrm{CARS}})^2$. The deviation of the factor $M$ from $0.123\,(l_{\mathrm{opt}}^{\mathrm{CARS}})^2$ increases with the growth in the phase mismatch $\Delta k$.

Phase mismatch reduces the optimal interaction length for the CARS process and lowers the maximum waveguide CARS enhancement attainable with a hollow microstructure fiber. The power of the CARS signal becomes an oscillating function of the fiber length under these conditions (Fig. 6a). The characteristic period of these oscillations is determined by the coherence length. Oscillations become less pronounced and then completely flatten out as optical losses build up (see also [91]). No oscillations are observed when the attenuation length becomes less than the coherence length (Fig. 6c). An important option offered by hollow microstructure fibers is the possibility to compensate for the phase mismatch related to the gas dispersion with an appropriate choice of waveguide parameters due to the waveguide dispersion component [61, 76].

### 2.8 Waveguide enhancement of nonlinear-optical processes in microstructure fibers: concluding remarks

Analysis performed in this section shows that hollow microstructure and photonic-crystal fibers allow coherent anti-Stokes Raman scattering to be substantially enhanced relative to the regime of tight focusing, as well as relative to waveguiding regimes in hollow solid-cladding fibers. Based on the analysis of waveguide losses, as well as phase-mismatch and group-delay effects, we have determined the optimal fiber lengths providing maximum waveguide enhancement for stimulated Raman and coherent anti-Stokes Raman scattering. Our analysis also reveals the existence of the physical limit for the waveguide enhancement of nonlinear-optical processes. Physically, this limit stems from the competition of diffraction and waveguide confinement of radiation due to the refractive-index step.

Optimal confinement of electromagnetic radiation, allowing maximum enhancement of nonlinear-optical processes, is achieved in submicron threadlike waveguiding channels with air cladding. Such waveguide structures with the maximum refractive-index step have been recently implemented in microstructure fibers. We have derived approximate asymptotic expressions that provide in several important cases an adequate qualitative understanding of the influence of fiber parameters on the optimal values of the fiber core radius and the maximum values of the waveguide enhancement factor and allow these quantities to be estimated with satisfactory accuracy.

The maximum CARS enhancement in a hollow microstructure fiber relative to the tight-focusing regime was shown to scale as $\lambda^2/\alpha^2 a^4$ with radiation wavelength $\lambda$, inner fiber radius $a$, and magnitude of radiation losses $\alpha$. Due to the rapid growth in CARS efficiency with a decrease in the inner radius of a hollow fiber, the limiting waveguide CARS enhancement factor in hollow microstructure fibers may substantially exceed analogous factors attainable with solid-cladding hollow fibers, as well as the waveguide enhancement for stimulated Raman scattering in hollow microstructure and photonic-crystal fibers. We have shown that the influence of group-delay effects on CARS and SRS in hollow fibers can be radically reduced, due to the dispersion of waveguide modes, with an appropriate choice of the gas pressure, the inner diameter of a hollow fiber, and the waveguide modes involved in the nonlinear-optical process.

Hollow-core microstructure and photonic-crystal fibers thus suggest the means for creating highly efficient gas sensors based on CARS spectroscopy, as well as SRS frequency converters. Waveguiding regimes supported by hollow-core photonic-crystal fibers allow the amount of sample gas required for spectroscopic analysis to be substantially reduced and provide an opportunity to perform nonlinear-optical experiments using low-power laser pulses.

## 3. Supercontinuum generation and frequency conversion of femtosecond pulses in microstructure fibers

In this section, we will consider different strategies of nonlinear-optical spectral transformation of femtosecond laser pulses in microstructure fibers. We will show that phase-matched four-wave mixing in higher-order modes of microstructure fibers allows high efficiencies of nonlinear-optical frequency conversion to be achieved for low-energy femtosecond laser pulses.

We will also discuss the results of experiments demonstrating highly efficient multiplex frequency conversion of unamplified subnanojoule femtosecond pulses of Ti:sapphire-laser radiation in fused silica microstructure fibers. Nonlinear-optical spectral transformation of femtosecond pulses in an array of fused silica threadlike channels in these microstructure fibers results in the generation of isolated anti-Stokes spectral components within the wavelength range of 400–500 nm. An efficiency of frequency conversion of about 20% can be achieved with the use of this method for 800-nm pump pulses with the energy 0.7 nJ and the pulse duration 70 fs. Applications of microstructure-fiber frequency converters in femtosecond photochemistry will also be discussed.

### 3.1 The frequency conversion problem and microstructure fibers

Frequency conversion of femtosecond laser pulses is one of the key issues in laser physics and quantum electronics. The standard solution to this problem is to use nonlinear-optical crystals [92]. Frequency-conversion capabilities of nonlinear crystals can be extended in certain cases by periodic poling, allowing quasi-phase matching of nonlinear optical interactions [93, 94]. The potential of photonic crystals for the frequency conversion of ultrashort pulses has been recently demonstrated, and several attractive recipes for the phase matching of nonlinear-optical processes have been suggested [95–97]. The main factors limiting the efficiency of frequency conversion of ultrashort pulses in nonlinear crystals and periodic structures include group-velocity dispersion and the limited spectral range of phase matching.

Microstructure [4–13] and tapered [51, 52] fibers possess several remarkable and unique properties, allowing highly efficient nonlinear-optical interactions to be implemented even for low-power ultrashort laser pulses. In particular, dispersion of such fibers can be tailored by changing their geometry [13]. A high refractive-index step between the core and the cladding, attainable with such fibers, provides a high degree of light confinement in the fiber core [14, 15]. Microstructure and tapered fibers offer much flexibility in phase-matching third-harmonic generation [16, 98] and four-wave mixing [17–21], allowing both radiation with a very broad spectrum (supercontinuum) [23–25] and isolated spectral components [19–21, 99, 100] to be generated with high efficiency.

We will demonstrate below that nonlinear-optical interactions in microstructure fibers may result in highly efficient frequency conversion of unamplified nano- and subnanojoule femtosecond Ti:sapphire-laser pulses. We will discuss the results of nonlinear-optical experiments performed with microstructure fibers integrating waveguiding channels and having the form of submicron fused silica threads. The difference in the geometric sizes of these channels gives rise to differences in their dispersion properties, permitting femtosecond pulses to be frequency-converted to different spectral ranges. Experimental studies described below reveal regimes of nonlinear-optical interactions where nano- and subnanojoule femtosecond Ti:sapphire-laser pulses generate isolated anti-Stokes spectral components lying within the wavelength range from 400 to 500 nm with an efficiency up to 20%.

### 3.2 Multiplex frequency conversion of unamplified femtosecond pulses

**3.2.1 Experimental technique.** Experiments on frequency conversion of unamplified femtosecond Ti:sapphire-laser pulses were performed with a family of fused silica microstructure fibers where the cladding consisting of several cycles of air holes surrounded the central fiber core with a diameter of a few micrometers (see the inset in Fig. 8). Microstructure fibers were fabricated of fused silica using the technology described in detail elsewhere [33, 101]. The minimal core diameter in the fabricated family of fibers was equal to 1 μm. The air-filling fraction of the microstructure part of the cladding in the created fibers, as can be seen from the inset in Fig. 8, is very high, providing a high refractive-index step between the core and the cladding in the fiber and strongly confining the light field to the fiber core.

An array of submicron-size fused silica channels in the form of threads, bounded by the system of air holes in the fiber cladding (see the inset in Fig. 8), serve as additional multiple cores of the fiber, providing a high degree of light confinement due to the high refractive-index step and allowing waveguide enhancement factors close to the physical limit [102], determined by the competition of diffraction and refractive-index-step waveguiding [103], to be achieved for nonlinear-optical processes.

Physically, the enhancement of nonlinear-optical processes in such an array of submicron fused silica waveguiding threads is due to the same factors as the enhancement of nonlinear-optical interactions in tapered fibers. This microstructure fiber design integrates several small-core high-refractive-index-step fused silica waveguide channels into a bundle. Such a fiber can be made as long as hundreds of meters [104], thus permitting length limitations, typical of tapered fibers, to be overcome by means of fiber microstructuring. The fact that the microstructure-integrated

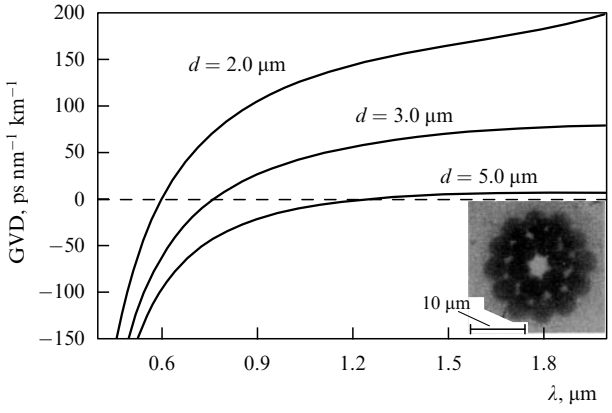


**Figure 8.** Group-velocity dispersion (GVD) calculated for the fundamental guided mode of a microstructure fiber with two cycles of air holes around the central waveguiding core with the diameter $d$. The inset shows the cross-section image of the microstructure fiber.

bundle includes submicron fused silica waveguiding threads with different sizes helps to achieve wavelength tunability in the frequency conversion of ultrashort pulses.

Our method of numerical analysis of guided modes in microstructure fibers was based on a modification of the approach proposed by Monro et al. [105–107]. The transverse distribution of the electric field in the cross section of a microstructure fiber was represented as an expansion in orthonormalized Hermite–Gauss polynomials. The two-dimensional profile of the refractive index squared in the cross section of the fiber, $n^2(x, y)$, was also represented as an expansion in Hermite–Gauss polynomials and a set of orthogonal periodic functions. Substituting these functional series into the wave equations reduces the vectorial problem we start with to an eigenfunction and eigenvalue problem for the relevant matrix equation. Solving this problem, we can find the propagation constants $\beta$ and spatial field and intensity distributions in waveguide modes.

Figure 8 displays the results of our calculations for the group-velocity dispersion (GVD) performed with the use of the above-described approach. Microstructure fibers with two cycles of air holes around the central fiber core with a diameter of about 3 μm provide, as can be seen from Fig. 8, an anomalous GVD regime for 800-nm Ti:sapphire-laser radiation. The wavelength of this radiation lies close to the zero-GVD point, which allows dispersion pulse spreading to be reduced and phase matching to be achieved for parametric four-wave mixing processes [19, 20] in such a fiber.

The laser system employed in our experiments was based on an argon-laser-pumped Ti:sapphire laser, which generated 50–80-fs pulses of 790–810-nm radiation with the pulse energy 0.2–5 nJ. The envelope and the spectrum, as well as the spectral phase and the chirp for these laser pulses at the input and at the output of the microstructure fiber were measured by means of spectral phase interferometry for direct electric-field reconstruction (SPIDER) [108]. The standard autocorrelation technique was also employed to assess the duration of laser pulses and the shape of their envelope. Spectral measurements were carried out with the use of an Ocean Optics spectrometer.

Radiation generated by the Ti:sapphire laser system was coupled into the central core or one of the threadlike fused silica channels (see the inset in Fig. 8) of a microstructure fiber, which was placed on a three-coordinate translation stage. To improve the coupling of pump radiation into the central core of the microstructure fiber, the Ti:sapphire-laser beam was focused with a standard LOMO-20 objective, providing a focused beam waist length of 6–8 μm. A LOMO-40 objective was employed to couple pump radiation into submicron threadlike fused silica channels. The waist length of the focused laser beam was equal to 3–4 μm in this case. The duration of input laser pulses measured with the use of the SPIDER and standard autocorrelation techniques was equal to 70–80 fs.

The initial chirp and the spectral phase of the pulse have a noticeable influence on the efficiency of nonlinear-optical processes in microstructure fibers [109]. We employed this effect to set a phase control of anti-Stokes generation by Ti:sapphire-laser pulses and to achieve maximum efficiencies of the frequency conversion of ultrashort pulses in a microstructure fiber. Typical chirp and spectral-phase profiles of Ti: sapphire-laser pulses measured with the use of the SPIDER technique at the input of the microstructure fiber are presented in the insets in Figs 9a and 9b.

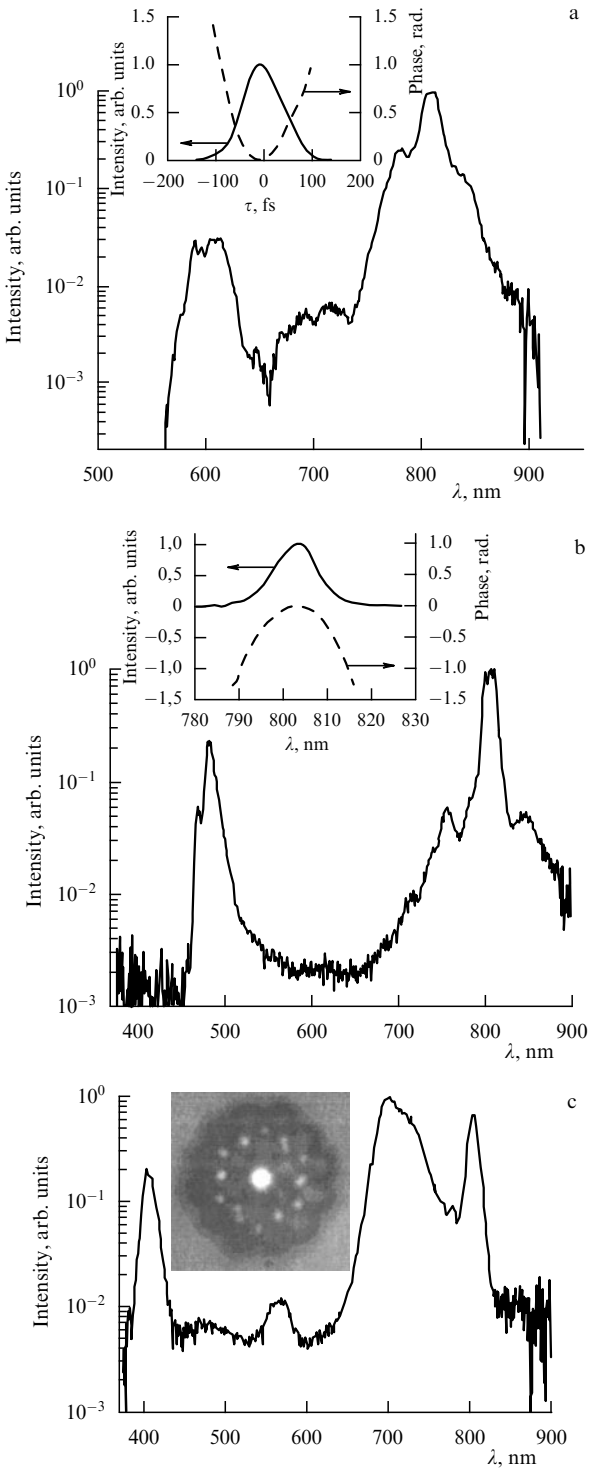


**Figure 9.** (a) The spectrum of radiation at the output of a microstructure fiber with the length 10 cm and a core diameter of about 3 μm. The input laser pulse has the central wavelength 800 nm, the energy 0.8 nJ, and the initial duration about 70 fs. The inset in Fig. 9a shows the envelope and the chirp of a femtosecond Ti:sapphire-laser pulse at the input of the microstructure fiber measured with the use of the SPIDER technique. (b, c) Nonlinear-optical frequency conversion of unamplified 0.7-nJ Ti:sapphire-laser pulses with the initial duration 70 fs in submicron channels of a microstructure fiber with the length 2 cm. The output spectrum features anti-Stokes components centered at (b) 490 and (c) 405 nm. The inset in Fig. 9b displays the spectrum and the spectral phase of a femtosecond Ti:sapphire-laser pulse at the input of the microstructure fiber measured with the use of the SPIDER technique.

**3.2.2 Four-wave mixing and multiplex frequency conversion.** Propagation of femtosecond laser pulses through microstructure fibers was accompanied by nonlinear-optical interactions, giving rise to new frequency components in the spectrum of radiation coming out of the fiber and supercontinuum generation. Figure 9a displays the spectrum of broadband emission produced by 70-fs 0.8-nJ pump pulses in the 3-μm central core of the microstructure fiber with the structure of cross section shown in the inset in Fig. 8. The length of the fiber used in this experiment was about 10 cm. Analysis of dispersion properties of this microstructure fiber (see Section 3.2.1) shows that supercontinuum is generated in these experiments in the regime of anomalous dispersion.

The main tendencies in the spectral transformation of femtosecond pulses and the properties of supercontinuum emission observed in these experiments generally agree well with the scenarios of supercontinuum generation due to soliton fission and parametric four-wave mixing [17, 18, 25]. The created microstructure fibers thus provide high-efficiency supercontinuum generation for unamplified subnanojoule femtosecond pulses of Ti:sapphire-laser radiation.

Nonlinear-optical spectral transformation of femtosecond Ti:sapphire-laser pulses in submicron fused silica waveguiding channels of different diameters (see the insets in Figs 8, 9c) gave rise to new frequency components within a broad spectral range. In particular, parametric four-wave mixing $2\omega_p = \omega_s + \omega_a$ (where $\omega_p$ is the frequency of pump radiation and $\omega_s$ and $\omega_a$ are the frequencies of the Stokes and anti-Stokes signals, respectively) resulted in the efficient generation of anti-Stokes components within the wavelength range of 400 – 500 nm (Figs 9b, 9c). Phase matching for such processes in microstructure fibers was analyzed in earlier works [17 – 20]. The wavelength range where the efficiency of nonlinear-optical frequency conversion reaches its maximum is determined by the dispersion properties of the waveguide channel. The size of the channel is thus the key parameter, controlling the process of nonlinear-optical frequency conversion.

The frequency tunability of new spectral components generated by unamplified femtosecond Ti:sapphire-laser pulses in submicron fused silica channels of different diameters is illustrated in Figs 9b and 9c. The spectrum of the output radiation presented in Fig. 9b features an intense anti-Stokes component centered at 490 nm. This component carries up to 20% of the output radiation energy. The central frequency of the anti-Stokes component generated in the microstructure fiber can be shifted by changing the diameter of the waveguiding channel.

Figure 9c displays the spectrum of the output radiation with an intense anti-Stokes component centered at approximately 405 nm. Generation of this component is accompanied by the build-up of a spectral component with the central wavelength of about 710 nm. The amplitude of this 710-nm frequency component in the output radiation spectrum exceeds the amplitude of the spectral component corresponding to pump radiation. Off the phase-matching condition, anti-Stokes components are either missing in the output spectra or produced with an extremely low efficiency. Femtosecond pump pulses also experienced noticeable spectral broadening due to self-phase modulation as they propagated through submicron channels of the microstructure fiber.

The experiments presented above demonstrate the possibility of creating highly efficient multicolor frequency converters for ultrashort laser pulses based on microstructure fibers. These fibers can implement a multiplex frequency conversion of subnanojoule femtosecond pulses with efficiencies exceeding those attainable with nonlinear crystals.

The inset in Fig. 9c shows the cross-section image of a microstructure fiber generating multiple colors by frequency-upconverting unamplified Ti:sapphire-laser pulses. The efficiency of nonlinear-optical frequency conversion in microstructure fibers is improved relative to nonlinear crystals due to large interaction lengths, typical of the waveguide regime, and the possibility of phase-matching an anti-Stokes signal of a given wavelength with pump radiation by creating a fiber with a required dispersion profile.

### 3.3 Frequency conversion of pulses produced by an optical parametric amplifier and wavelength-tunable supercontinuum generation

In this section, we will show that phase-matched four-wave mixing in microstructure fibers of the above-described design allows high efficiency in anti-Stokes frequency conversion to be achieved for wavelength-tunable nano- and subnanojoule femtosecond laser pulses produced by an optical parametric amplifier (OPA). Ultrashort pulses of OPA radiation can also be employed to efficiently generate frequency-tunable supercontinuum emission.

The results of experimental studies [20], devoted to the nonlinear-optical spectral transformation of OPA pulses, are presented in Figs 10 and 11. In these experiments, 70-fs OPA laser pulses of 790-nm radiation with an energy of 0.01 – 3 nJ were coupled into the central core or one of the submicron waveguide channels of a microstructure fiber with the structure of cross section shown in inset *1* in Fig. 10a. Four-wave mixing processes in such fibers result in the efficient generation of new spectral components. Analysis of the beam pattern of the anti-Stokes signal produced in the central core of the microstructure fiber (the inset in Fig. 10b) reveals a spatial structure characteristic of a higher-order waveguide mode.

Theoretical analysis of the dispersion properties of guided modes supported in the central core of the studied microstructure fibers (see Section 3.2.1) indicates the possibility of phase-matching parametric four-wave mixing $2\omega_p = \omega_s + \omega_a$, where $\omega_p$ is the frequency of pump radiation and $\omega_s$, $\omega_a$ are the frequencies of the Stokes and anti-Stokes signals, respectively. Figure 10a displays the mismatch $\delta\beta$ of the propagation constants for such a parametric process in the fundamental and higher-order waveguide modes (the structure of modes is shown in the insets in Fig. 10a). Phase matching can be achieved for the 800-nm pump and the anti-Stokes signal generated in a higher-order waveguide mode within the range of wavelengths of 520 – 530 nm. The propagation-constant mismatches for such parametric four-wave mixing involving 800- and 790-nm pump are shown by curves *1* and *2* in Fig. 10a.

The amplitude of the anti-Stokes signal, as shown by experiments [20], increases with the growth in the intensity of the pump pulse (Fig. 10b). The anti-Stokes signal amplitude starts to exceed the amplitude of the pump component in the output spectrum for an input pump pulse energy of about 0.5 nJ. As the pump pulse broadens, due to self-phase modulation, with the increase in the pump intensity, shorter-wavelength components appear in the spectrum of the pump pulse (curves *2 – 4* in Fig. 10b). These components of the pump are phase-matched with higher frequency anti-Stokes

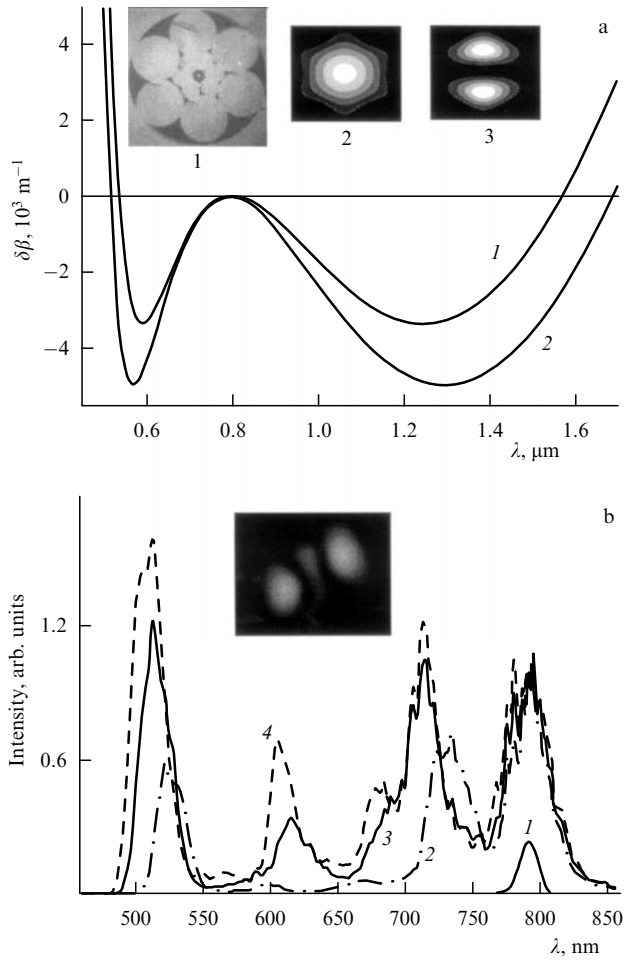


**Figure 10.** (a) Mismatch of the propagation constants $\delta\beta$ of higher-order waveguide modes involved in the FWM process $2\omega_p = \omega_s + \omega_a$ in a fused silica microstructure fiber with the core diameter 4.8 μm. The pump wavelength is 800 nm (curve *1*) and 790 nm (curve *2*). Inset 1 shows the cross-sectional view of the microstructure fiber. Insets 2 and 3 display field intensity distributions in the fundamental and higher order guided modes. (b) Spectral transformation of a 70-fs pulse of 790-nm pump radiation in a microstructure fiber with a 4.8-μm-diameter central core [20]. The spectrum of the input pulse is shown by curve *1*. The input pulse energy is (*2*) 0.1 nJ, (*3*) 0.5 nJ, and (*4*) 1 nJ. The inset shows the emission pattern at the output of the fiber.

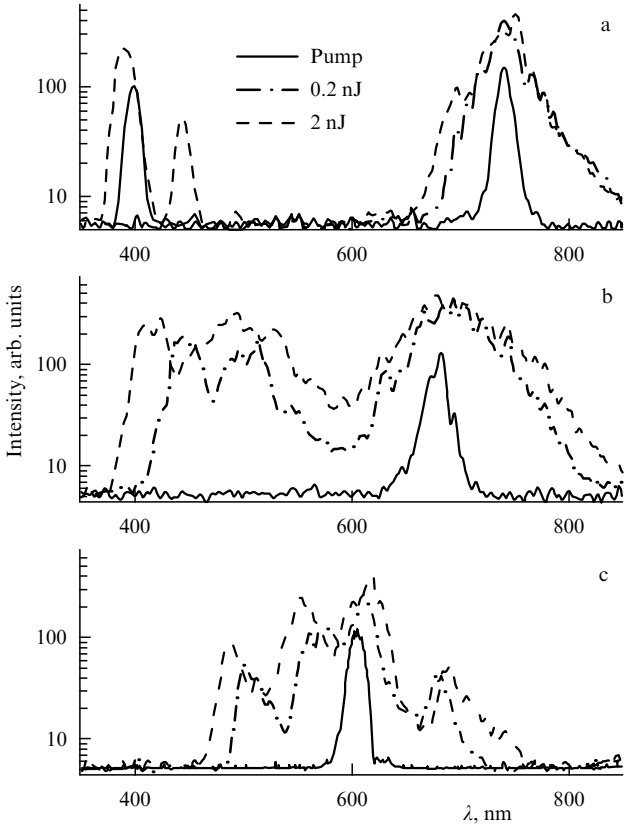


**Figure 11.** Spectra of supercontinuum emission produced [20] by 80-fs pulses of OPA radiation with the wavelength tuned from 750 to 600 nm in the 0.8-μm waveguide channel of a microstructure fiber with the cross-section structure shown in inset 1 in Fig. 8 and the length 2.5 cm.

wavelengths, leading to the blue shift in the anti-Stokes signal relative to the wavelength of 520 nm [20]. This effect can be employed to tune the frequency of the nonlinear signal generated in a microstructure fiber.

Dispersion of peripheral submicron channels in the considered microstructure fiber differs from the dispersion of the central core, allowing the frequency of femtosecond pulses to be converted to other spectral ranges. Due to the high refractive-index step between fused silica and the air, these submicron channels strongly confine guided modes of electromagnetic radiation, allowing, as shown in Section 2 of this paper, the physical limit of waveguide enhancement of nonlinear-optical processes to be attacked.

Figure 11 illustrates how the wavelength of input radiation influences the spectra of radiation detected at the output of the microstructure fiber. As can be seen from this figure, femtosecond pulses of 750-nm radiation coupled into 0.8-μm waveguide channels of the microstructure fiber efficiently generate an anti-Stokes signal of around 400 nm (Fig. 11a) in the fundamental guided mode, with the frequency interval between the anti-Stokes and pump signals being about 350 THz. For 1.5-nJ pump pulses coupled into the submicron core of a 2.5-cm-long MS fiber, the ratio of the anti-Stokes signal amplitude to the amplitude of pump radiation is approximately equal to 0.5, with allowance for the frequency dependence of the detector sensitivity.

Peripheral submicron channels allow the efficiency of supercontinuum generation to be improved relative to the central fiber core. With the pump wavelength $\lambda_p$ lying far from the wavelength of zero group-velocity dispersion $\lambda_0$ (around 510 nm for the fundamental mode of 0.8-μm-diameter fused silica waveguide channels), a noticeable gap between the pump and the anti-Stokes part of the output spectra was observed (Fig. 11a).

Emission of anti-Stokes components of around 400 nm under these conditions agrees well with the soliton-fission and four-wave mixing scenarios of supercontinuum generation in microstructure fibers [17, 18]. Tuning the pump wavelength $\lambda_p$ closer to $\lambda_0$, we observe that the self-phase-modulation-broadened pump and the anti-Stokes signal merge into a broad continuous spectrum (Figs 11b, 11c), resulting in a bright white-light emission coming out of the microstructure fiber.

### 3.4 Nonlinear-optical spectral transformation of femtosecond Cr:forsterite-laser pulses

In this section, we will discuss the results of experiments demonstrating highly efficient generation of frequency-

tunable radiation within the wavelength range of 350 – 600 nm through nonlinear-optical frequency conversion of femtosecond pulses of a Cr:forsterite laser in an array of submicron threadlike fused silica waveguiding channels in a microstructure fiber. Nonlinear-optical spectral transformation of femtosecond pulses in such waveguide channels may result in the generation of isolated spectral components with frequencies exceeding the frequency of the third harmonic. The interval between the pump frequency and the frequency of the nonlinear signal under these conditions may exceed 580 THz.

Experiments [100] on the frequency conversion of femtosecond Cr:forsterite-laser pulses were performed with the fused silica microstructure fibers described in Section 3.2.1 (see the insets in Figs 8, 12a). An array of submicron-size fused silica waveguide channels in the form of threads serve as additional multiple cores of microstructure fibers. These channels have different diameters, which helps to achieve wavelength tunability in the frequency conversion of ultrashort pulses (femtosecond pulses of a Cr:forsterite laser in the experiments described in this section).

The laser system employed in experiments [100] consisted of a $Cr^{4+}$: forsterite master oscillator, a stretcher, an optical isolator, a regenerative amplifier, and a compressor. The master oscillator, pumped with a fiber Nd:YAG laser, generated 30 – 50-fs light pulses with a repetition rate of 120 MHz. Nonlinear-optical experiments were performed with laser pulses having the central wavelength 1270 nm, the bandwidth 26 nm, and a mean power of about 180 mW.

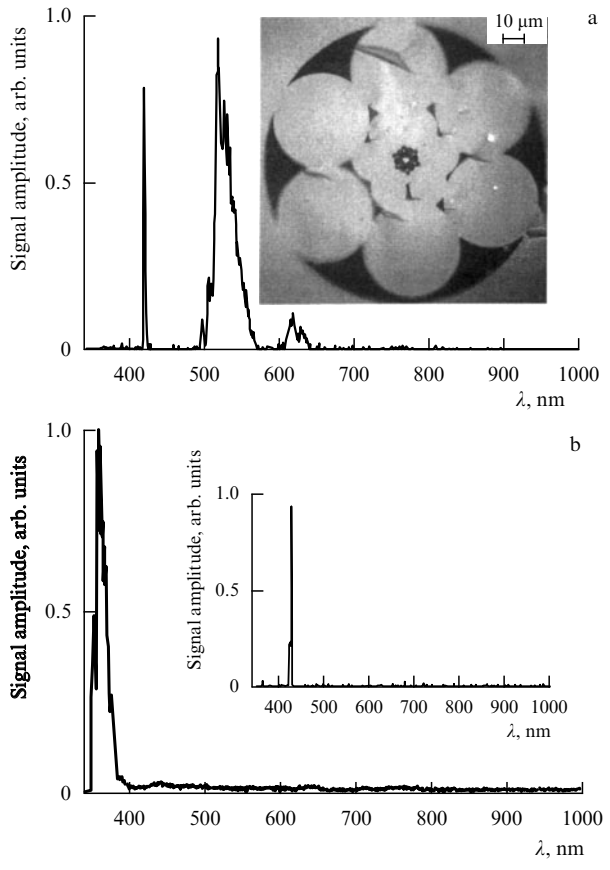


**Figure 12.** (a) Generation of anti-Stokes radiation and the third harmonic in the central core of a microstructure fiber with a diameter of 3 μm. The inset shows the cross-section image of the microstructure fiber with a single cycle of air holes around the central waveguiding core. (b) Generation of a high-frequency spectral component with the wavelength around 370 nm in a submicron threadlike waveguiding channel of the microstructure fiber. The fiber length is 7 cm. The energy of laser pulses coupled into the fiber is about 50 nJ. The inset presents the spectrum of the third harmonic generated in submicron waveguiding channels of the microstructure fiber.

Radiation generated by the Cr:forsterite laser system was coupled into the central core or one of the threadlike fused silica channels (see the inset in Fig. 8) in a microstructure fiber. A standard LOMO-20 objective was used to excite guided modes in the central core of the microstructure fiber. The waist length of the laser beam focused by this objective was equal to 6 – 8 μm. A LOMO-40 objective was employed to couple radiation into submicron threadlike channels of the microstructure fiber. The waist length of the focused laser beam was equal to 3 – 4 μm in this case. The duration of laser pulses at the input of microstructure fibers was about 150 fs. Spectral measurements were performed with an Ocean Optics spectrometer.

Propagation of femtosecond laser pulses through microstructure fibers was accompanied by wave mixing, giving rise to new frequency components in the spectrum of radiation coming out of the fiber. Parametric four-wave mixing $2\omega_p = \omega_s + \omega_a$ (where $\omega_p$ is the frequency of pump radiation and $\omega_s$ and $\omega_a$ are the frequencies of the Stokes and anti-Stokes signals, respectively) in the central fiber core resulted in the efficient generation of anti-Stokes radiation of around 530 nm with a spectral bandwidth of about 35 nm (Fig. 12a). Efficient generation of the third harmonic of pump radiation was also observed with the amplitude of the third harmonic comparable to the amplitude of the anti-Stokes signal (see the inset in Fig. 12b).

Nonlinear-optical spectral transformation of femtosecond Cr:forsterite-laser pulses in submicron fused silica waveguiding channels of different diameters resulted in the generation of new frequency components within a broad spectral range (Fig. 12). The possibility of tuning the frequencies of new spectral components generated by femtosecond Cr:forsterite-laser pulses in submicron fused silica channels of different diameters is illustrated in Fig. 12.

An array of microstructure-integrated submicron fused silica channels implemented in our fibers provides a unique possibility of converting the frequency of femtosecond Cr:forsterite-laser pulses to the range of wavelengths shorter than the wavelength of the third harmonic. Effective cascading of nonlinear-optical processes in submicron waveguiding channels leads, as can be seen from Fig. 12b, to the generation of the frequency component with the central wavelength around 370 nm and a spectral bandwidth of about 30 nm (the wavelength of the third harmonic is 420 nm for Cr:forsterite-laser radiation). This process increases the carrier frequency of femtosecond pulses by more than 580 THz.

The efficiency of this frequency-conversion process was as high as several percent, giving rise to 370-nm emission in the form of blue light easily seen with the naked eye on a white screen. The developed microstructure fiber design thus allows femtosecond Cr:forsterite-laser pulses to be frequency-converted to the spectral range that is of special interest and importance for photochemical and photobiological studies, enhancing the capabilities of femtosecond Cr:forsterite lasers in femtosecond spectroscopy and time-resolved measurements, as well as extending the applicability area of such laser systems to the control of ultrafast processes in physics, chemistry, and biology.

### 3.5 Frequency conversion of unamplified femtosecond pulses in microstructure fibers for photochemical applications

In this section, we will consider one of the applications of nonlinear-optical frequency converters of ultrashort pulses based on microstructure fibers. We will show that microstructure fibers can frequency-upconvert femtosecond pulses to the spectral range where laser radiation efficiently initiates photochemical processes, including photochromism. We will discuss the results of experiments demonstrating that microstructure fibers with a specially designed dispersion profile convert the frequency of unamplified subnanojoule femtosecond Ti:sapphire-laser pulses to the anti-Stokes range, generating radiation with a wavelength around 400 nm. This anti-Stokes radiation is then used to initiate a photochromic reaction in a solid-phase polymer sample containing spiropyran molecules.

Photochromism [111 – 113] is defined as a light-induced reversible transformation in chemical species between two relatively stable forms having different absorption spectra. This phenomenon is often routinely understood as light-induced change of color, well-known in every-day life through sunglasses that darken under the action of sunlight and recover their color in the presence of scattered light.

Applications of photochromism, which has been known since the 19th century [114], include self-developing photography, optical switching and filtering [111, 112], three-dimensional optical data storage [115, 116], and, recently, reversible waveguide writing [117, 118], microfabrication of telecommunication and photonic components [119], and engineering of photoswitchable biomaterials [120].

Experiments [34] demonstrating the potential of unamplified femtosecond pulses frequency-upconverted in microstructure fibers for photochromism initiation were performed with polymethyl methacrylate (PMMA) samples doped with spiropyran molecules (shown in the inset in Fig. 13). The concentration of spiropyran in a $9 \times 9 \times 10$ mm$^3$ sample was $1.6 \times 10^{-2}$ mol l$^{-1}$. Spiropyran molecules in the uncolored form (form *A*) efficiently absorb radiation with wavelengths shorter than 410 nm. The photochromic effect, occurring through C – O bond cleavage, transforms form-*A* spiropyran molecules into a colored, merocyanine-isomer form (form *B*), giving rise to a broad absorption band in the visible region.

The laser system employed in experiments [34] was based on an argon-laser pumped Ti:sapphire laser (Fig. 13), which generated 80-fs pulses of 800-nm radiation with a pulse energy of 0.3 nJ. These pulses were coupled into a microstructure fiber where the cladding included two cycles of air holes surrounding the central fiber core with a diameter of about 3 μm. The cross-section view of the microstructure fiber used in these experiments is shown in the inset in Fig. 8. An array of submicron-size fused silica channels in the form of threads, bounded by a system of air holes in these microstructure fibers, served for the frequency conversion of unamplified femtosecond pulses.

The wavelength of the anti-Stokes signal generated in peripheral submicron waveguide channels under these conditions is determined by the dispersion properties of guided modes involved in the nonlinear-optical process. The transverse size of a waveguide channel is thus the key parameter, controlling the color of the anti-Stokes signal. Fused silica waveguiding channels with different sizes built into the considered microstructure fibers help to achieve wavelength tunability in the anti-Stokes frequency conversion of femtosecond pulses.

Figure 14 shows the spectra of radiation coming out of two different channels in the microstructure fiber, displaying intense anti-Stokes components. One of these anti-Stokes signals (the blue line) has a spectrum with the maximum around 405 nm (Fig. 14a). The spectrum of the second anti-Stokes signal (the green line) peaks around 490 nm (Fig. 14b). The blue anti-Stokes line falls within the absorption band of the uncolored form of spiropyran compounds and can be used to initiate photochromism in spiropyran/PMMA samples. The green anti-Stokes line lies within the absorption band characteristic of form-*B* spiropyran. This component can be employed to induce the reverse photochromic transformation, recovering the uncolored, form-*A* spiropyran.

Comparison of the spectra of the blue anti-Stokes line at the input (line *1* in inset 1 in Fig. 14a) and at the output (line *2* in the same inset) of the spiropyran/PMMA sample shows that this line is ideally suited to transform spiropyran molecules from form A to form B. The short-wavelength part of the anti-Stokes signal is almost completely absorbed by the photochromic material, while the long-wavelength

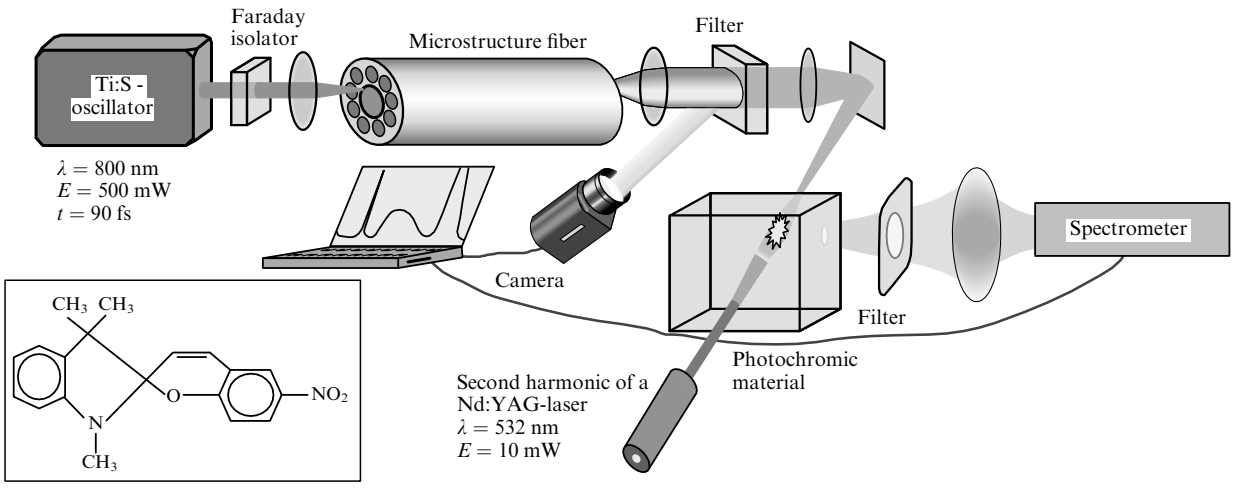


**Figure 13.** Laser setup for the frequency upconversion of unamplified femtosecond laser pulses in microstructure fibers adapted to photochromism initiation. The inset shows the structure formula of a spiropyran molecule.

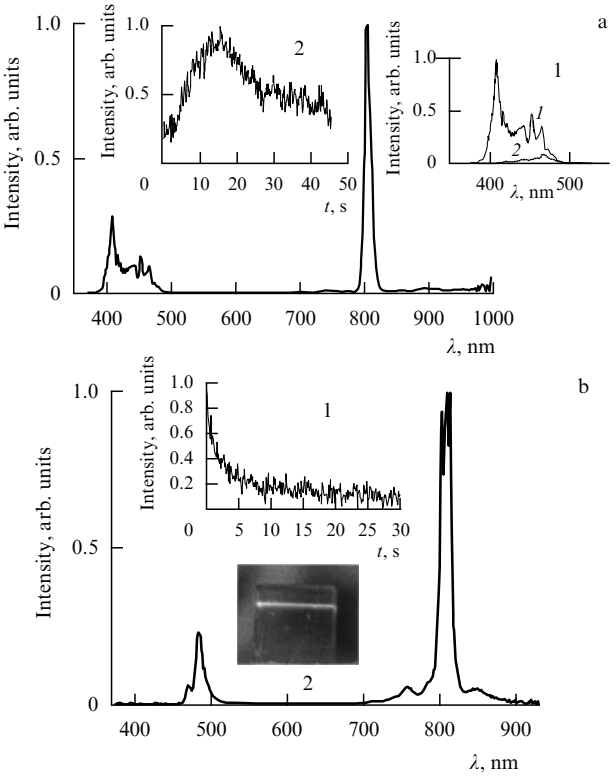


**Figure 14.** Generation of the blue (a) and green (b) anti-Stokes lines in submicron channels of a 5-cm-long microstructure fiber (cross-section view of this fiber is shown in the inset in Fig. 8) by 0.3-nJ, 80-fs pulses of 800-nm radiation. Inset 1 in Fig. 14a shows the spectra of the blue anti-Stokes line at the input (curve *1*) and at the output (curve *2*) of the spiropyran/PMMA sample. Inset 2 in Fig. 14a presents the kinetics of the photoluminescence (PL) signal, visualizing the generation of form-*B* spiropyran in the spiropyran/PMMA sample by the blue anti-Stokes line produced in the microstructure fiber. Inset 1 in Fig. 14b displays the decay of the photoluminescence signal, indicating the recovery of form-A spiropyran under the action of the green anti-Stokes line in the area pre-irradiated with the blue anti-Stokes line, switched off at $t = 0$. Inset 2 in Fig. 14b features photoluminescence excited by the green anti-Stokes line, visualizing micromachining of a photochromic material by femtosecond Ti:sapphire-laser pulses through two-photon photochromism.

part of the spectrum is absorbed less efficiently, indicating that, with such an emission spectrum, we are still able to avoid undesirable absorption of radiation by form-B spiropyran, stimulating the reverse photochromic reaction.

Absorption of the blue anti-Stokes line generated in the microstructure fiber initiates the photochromic processes in spiropyran molecules, resulting in the formation of merocyanine isomers. This photochromic transformation, leading to the accumulation of form-*B* spiropyran, is visualized by characteristic photoluminescence (PL) within the spectral range of 600 – 700 nm excited with 532-nm second-harmonic radiation from a diode-pumped 10-mW continuous-wave Nd : YAG laser (see Fig. 13). Radiation of this laser also stimulates the reverse photochromic transformation, recovering form-*A* spiropyran in the sample, thus preventing the gradual pulse-to-pulse accumulation of form-*B* spiropyran in the laser-irradiated area.

As the Ti:sapphire laser is switched on (at the moment $t = 0$ in inset 2 in Fig. 14a), the blue anti-Stokes line produced in the microstructure fiber starts to generate form-*B* spiropyran in the photochromic sample, visualized by the growth in photoluminescence intensity as a function of time. With the Ti:sapphire laser switched off (at the moment $t = 16$ s in inset 2 in Fig. 14a), the photoluminescence signal decays, indicating the recovery of form-A spiropyran in the sample under the action of 532-nm second-harmonic radiation of the continuous-wave Nd:YAG laser.

The green anti-Stokes line induces the reverse photochromic transformation. The decay of the photoluminescence signal in inset 1 in Fig. 14b shows how this emission line recovers form-A spiropyran in the area of the photochromic sample previously colored by the blue anti-Stokes line, which is switched off at $t = 0$. The photoluminescence excited by the green anti-Stokes line, as shown in inset 2 in Fig. 14b, can be employed to visualize 3D microstructures and waveguides written in a photochromic material by femtosecond Ti:sapphire-laser pulses through two-photon-absorption-induced photochromism.

Experiments presented here demonstrate that microstructure fibers radically enhance the capabilities of basic femtosecond lasers without amplification stages. In the experiments discussed above, microstructure-integrating arrays of submicron fused silica waveguide channels have been employed for efficient anti-Stokes frequency conversion of unamplified femtosecond Ti:sapphire-laser pulses with an energy of about 0.3 nJ.

Anti-Stokes radiation generated in microstructure fibers allows photochromism initiation in solid-phase polymer samples containing spiropyran molecules. Microstructure fibers are thus shown to provide high efficiencies of frequency conversion of unamplified femtosecond pulses to the spectral range where frequency-converted ultrashort pulses can be employed to initiate and control photochemical and photobiological processes.

### 3.6 Frequency conversion using microstructure fibers: concluding remarks

Experiments presented in this section demonstrate highly efficient nonlinear-optical frequency conversion of unamplified femtosecond pulses in fused silica microstructure fibers. We have designed, fabricated, and tested in nonlinear-optical experiments microstructure fibers with waveguiding channels in the form of submicron fused silica threads. The size of a waveguiding channel is the key parameter for the spectral transformation of ultrashort laser pulses. This parameter determines dispersion properties of guided modes, thus controlling the frequencies of new spectral components generated as a result of nonlinear-optical frequency conversion of ultrashort laser pulses. The possibility of tuning the frequencies of such new anti-Stokes spectral components has been experimentally demonstrated by coupling femtosecond pulses of Ti:sapphire- and Cr:forsterite-laser radiation into submicron fused silica waveguiding channels with different diameters. An efficiency of frequency conversion of about 20% was achieved for 800-nm pump pulses with the energy 0.7 nJ and the pulse duration 70 fs.

Dispersion optimization of guided modes in the central core of the created microstructure fibers allowed a high efficiency of supercontinuum generation to be achieved for unamplified Ti:sapphire-laser pulses. The proposed and implemented architecture of microstructure-integrated submicron fused silica waveguiding channels is thus shown to permit efficient multiplex frequency conversion of femtosecond Ti:sapphire- and Cr:forsterite-laser pulses to the spectral range that is of special interest and importance for photochemical and photobiological applications, suggesting

new solutions for femtosecond spectroscopy and the control of ultrafast processes in physics, chemistry, and biology.

## 4. Mode structure and spectral properties of supercontinuum emission from microstructure fibers

In this section, we will examine the mode structure and spectral properties of supercontinuum emission generated by femtosecond pulses of Ti:sapphire-laser radiation in microstructure fibers. We will present the results of experimental studies demonstrating that the long-wavelength (720 – 900-nm) and visible (400 – 600-nm) parts of supercontinuum radiation are spatially separated in microstructure-fiber modes, which can be isolated with an appropriate spectral filtering. The spatial modes thus isolated in spectrally sliced supercontinuum emission possess a spatial quality sufficient for efficient further frequency conversion. The possibility of achieving a high spectral quality of supercontinuum emission will be also demonstrated. Supercontinua produced in microstructure fibers will be shown to offer new approaches to designing a new generation of optical parametric amplifiers and broadband radiation sources for spectroscopic, metrological, and biomedical applications.

### 4.1 Supercontinuum generation in microstructure fibers

Supercontinuum (SC) generation [121] is a nonlinear-optical phenomenon involving spectral superbroadening of a light pulse resulting from the joint action of the whole catalogue of nonlinear-optical effects, such as self- and cross-phase modulation, four-wave mixing, and stimulated Raman scattering, often accompanied by soliton formation and propagation, as well as modulation instabilities.

As demonstrated recently, supercontinuum generation can be radically enhanced with the use of microstructure fibers [4 – 13]. Due to their remarkable properties, microstructure fibers make nonlinear optics accessible even to unamplified femtosecond pulses. Enhancement of a broad class of nonlinear-optical phenomena [7], accompanying the propagation of femtosecond pulses in microstructure fibers, makes it possible to generate supercontinuum radiation [23 – 26] starting with nano- and even subnanojoule energies of laser radiation.

Investigations of supercontinuum generation in microstructure fibers have revealed several interesting physical phenomena related to the nonlinear-optical interactions of ultrashort light pulses, providing deeper insights into the scenarios of spectral superbroadening of such pulses in different regimes of waveguiding in microstructure fibers [23 – 26]. The range of applications of supercontinuum generation in microstructure fibers is rapidly expanding, leading to revolutionary changes in optical metrology [27 – 31], opening new horizons in optical coherence tomography [32], and suggesting new solutions for the creation of compact and practical sources of broadband emission based on supercontinuum generation in microstructure fibers [33].

It would be very important, in view of the numerous spectroscopic, metrological, and tomographic applications of supercontinua generated in microstructure fibers, not only to improve the reproducibility and stability of the temporal characteristics and the spectral content of supercontinuum emission, but also to ensure a high spatial mode quality of this emission. In many practically important cases, highly efficient supercontinuum generation in microstructure fibers involves multimode-phase-matched four-wave mixing. Supercontinua are also emitted in the multimode regime under these conditions.

In this section, we discuss a method of spatial filtering and spectral slicing of supercontinuum radiation generated in a microstructure fiber with a small core diameter, where multimode-phase-matched four-wave mixing results in a preferable generation of new spectral components emitted as part of the supercontinuum in a certain (possibly high-order) guided mode. The results of experimental studies presented below in this section demonstrate the possibility of achieving a high spectral quality of supercontinua produced in microstructure fibers. We will explore the ways to control the spectrum of supercontinuum emission by matching the parameters of the pump pulse with the parameters of the microstructure fiber and by varying the initial chirp of the pump pulse. Based on these results, we will show that supercontinua produced in microstructure fibers offer new approaches to designing a new generation of optical parametric amplifiers and broadband radiation sources for spectroscopic, metrological, and biomedical applications.

### 4.2 Experimental aspects of supercontinuum generation

Experiments on supercontinuum generation were performed with a family of microstructure optical fibers where the cladding consisted of one, two, or more hexagonal cycles of air holes. A system of smaller auxiliary air holes in the cladding of such fibers improves the confinement of the light field to the fiber core (see the insets in Figs 8, 12a). Experimental studies confirm that the increase in the number of cycles of air holes around the fiber core reduces the magnitude of fiber losses. Optical losses have been determined for the microstructure fibers of the considered type from the results of measurements [122] performed on 100-m fiber segments. The magnitude of optical losses was estimated to be $2-3$ dB m$^{-1}$ for fibers with a single hexagonal cycle of air holes in the cladding and $0.4-0.5$ dB m$^{-1}$ for fibers with two cycles of air holes.

Spectral broadening and supercontinuum generation in microstructure fibers were studied in experiments [123] with the use of femtosecond pulses produced by a Ti:sapphire-laser system. This laser system included a Ti:sapphire master oscillator and a regenerative amplifier and was capable of generating 40-fs pulses of 800-nm radiation with an energy of up to 0.2 mJ per pulse and a repetition rate of 1 kHz. The energy of laser pulses coupled into the fiber ranged from 0.1 up to 50 nJ. Experiments were performed with fiber samples with lengths of $4-200$ cm. The laser beam was focused onto the input end of the fiber sample, placed on a three-dimensional translation stage, with a microobjective. Radiation coming out of the fiber was collimated with an identical microobjective and was split into two beams. One of these beams was delivered to a spectrograph, while the other was used to visualize the transverse intensity distribution in the emission coming out of the MS fiber by imaging the output end of the fiber onto a CCD camera.

### 4.3 Mode structure of supercontinuum radiation

Propagation of femtosecond laser pulses through a microstructure fiber was accompanied by a considerable spectral broadening of these pulses. With only a few nanojoules of Ti:sapphire-laser radiation coupled into a microstructure fiber sample with a length of several centimeters, generation of supercontinuum radiation with the spectral bandwidth

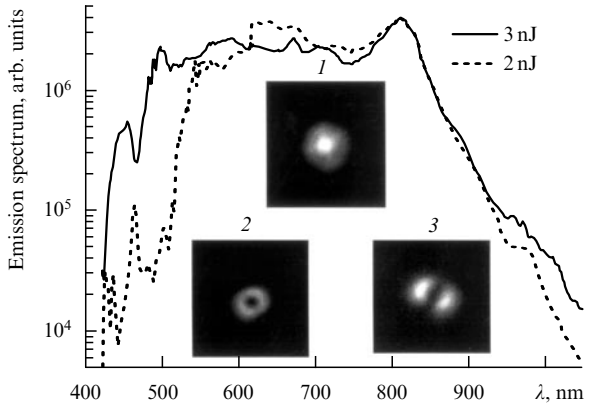


**Figure 15.** Spectra of supercontinuum emission excited by 40-fs pulses with an energy of 2 nJ (dotted curve) and 3 nJ (solid curve) in a 1.5-m microstructure fiber with a single cycle of air holes around the fiber core (see the inset in Fig. 12a) and a core diameter of 3 μm. The insets show transverse intensity distributions of supercontinuum radiation for the spectral range of (inset 1) 720 – 900 and (insets 2, 3) 400 – 600 nm.

exceeding an octave was observed. Figure 15 shows typical spectra of supercontinuum radiation generated by 40-fs pulses of Ti:sapphire-laser with an energy of 2 nJ (dotted curve) and 3 nJ (solid curve) in a 1.5-m microstructure fiber with a single cycle of air holes around the fiber core with the diameter 3 μm.

Supercontinuum radiation was generally produced in the multimode regime in our experiments. However, it was possible to filter isolated spatial modes for different spectral ranges of supercontinuum emission using a set of color-glass filters. The insets in Fig. 15 present typical results of such experiments performed for a supercontinuum generated in a 1.5-m-long microstructure fiber with a single cycle of air holes around the fiber core with the diameter 3 μm. The transverse intensity distribution of supercontinuum radiation measured with a filter providing maximum transmission within the range of 720 – 900 nm (inset 1 in Fig. 15) has a bell-like shape, displaying a single maximum on the beam axis. The visible part of supercontinuum radiation (400 – 600 nm), on the other hand, has a doughnut-like spatial mode structure (inset 2 in Fig. 15) under the same experimental conditions.

With a slight variation in the initial conditions of mode excitation at the input end of the microstructure fiber, the doughnut mode of the visible part of supercontinuum radiation (inset 2 in Fig. 15) was transformed into a more complicated, two-lobe pattern, shown in inset 3 in Fig. 15. Both the doughnut-like and the two-lobe modes remained reproducible and stable and were observed for microstructure fibers with lengths ranging from 20 up to 200 cm. Apparently, because of the poorer spatial overlapping between the pump beam and the two-lobe mode, the short-wavelength part of supercontinuum radiation in the case of the two-lobe mode was much less intense than in the case of the doughnut mode.

Physically, the idea of using microstructure fibers with small fiber cores for the generation of supercontinuum radiation that could be spectrally sliced into separated spatial modes is based on the fact that the difference between propagation constants for adjacent fiber modes supported by the fiber at a certain frequency increases with a decrease in the fiber core radius. Within the framework of the elementary theory of optical fibers [1], the relation between the difference of propagation constants $\Delta\beta$ characterizing two adjacent guided modes in a fiber and the fiber core radius $a$ is given by

$$\Delta\beta \approx \frac{\pi^2 c f_n}{4a^2\omega n_{\text{core}}},$$

where $c$ is the speed of light, $\omega$ is the radiation frequency, $f_n$ is a function of the mode index, and $n_{\text{core}}$ is the refractive index of the fiber core. This elementary relation is very instructive, however, as it explains in a very simple way why microstructure fibers with small core diameters may generate mode-separable supercontinuum radiation when FWM processes are phase-matched only for a certain spatial mode of the nonlinear signal generated through FWM for each supercontinuum slice (or at least for some of the supercontinuum slices).

Experimentally observed transformations of the spatial distribution of supercontinuum radiation (Fig. 15) indicate changes in multimode phase matching for FWM processes contributing to spectral superbroadening within different spectral ranges. Measurements performed on microstructure fibers with core diameters of 3 μm also show that phase matching is achieved only for a certain spatial mode of the emitted signal within each of the studied spectral ranges. This circumstance allows isolated spatial modes to be separated by spectrally slicing the supercontinuum emission.

### 4.4 Nonlinear-optical frequency conversion of spectrally sliced supercontinuum radiation and cross-correlation measurements

Frequency convertibility of a spectrally sliced supercontinuum is an important criterion of the quality of spatial modes of supercontinuum radiation. Based on this criterion, we can also judge whether supercontinuum radiation generated in microstructure fibers and spectrally sliced with the use of the above-described technique can be employed in practice for spectroscopic studies and pump – supercontinuum probe measurements.

With these circumstances in mind, we experimentally assessed the efficiency of nonlinear-optical frequency conversion for spectrally sliced spatial modes of supercontinuum radiation produced in a microstructure fiber. The sum-frequency signal was produced in our experiments by mixing different parts of supercontinuum radiation with the fundamental radiation of the above-described Ti:sapphire laser in a 100-μm-thick LBO crystal. Figure 16 presents the results of these measurements performed with the use of the long-wavelength part (720 – 900 nm) of the supercontinuum radiation (its spectrum is shown by curve *1* in Fig. 16a) mixed with the fundamental radiation of the Ti: sapphire laser in the LBO crystal in the noncollinear geometry of sum-frequency generation (SFG).

A broadband sum-frequency signal was produced within the spectral range from 370 to 430 nm in the direction determined by phase-matching conditions (see diagram 1 in Fig. 16). This geometry of sum-frequency generation allowed the efficiency of frequency conversion of about 0.1% to be achieved. We also observed collinear second-harmonic generation (SHG) using the long-wavelength part of supercontinuum radiation as a pump (see diagram 2 in Fig. 16). The efficiency of this second-harmonic generation under our experimental conditions was more than an order of magnitude lower than the efficiency of noncollinear sum-frequency generation (the relative efficiencies of SFG and SHG processes are shown on the left-hand side of Fig. 16).

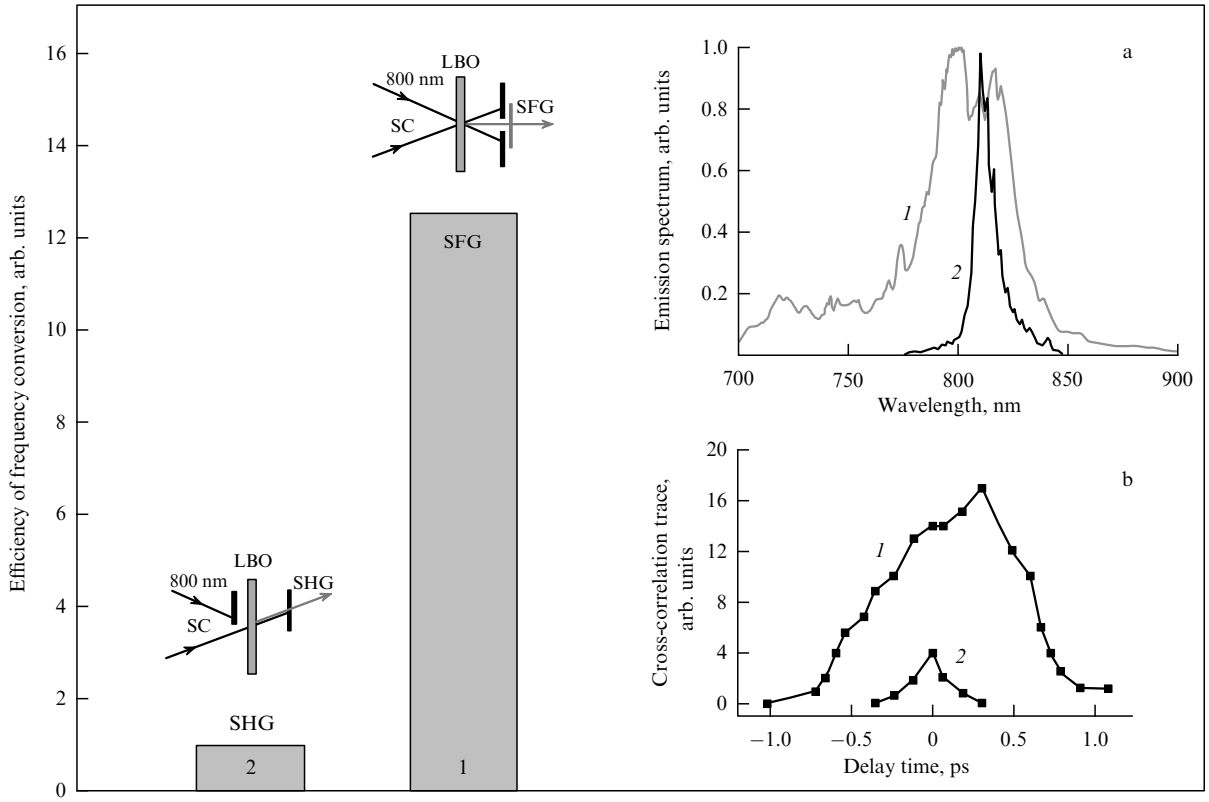


**Figure 16.** (a) The spectrum of supercontinuum (SC) radiation produced within the range of wavelengths from 720 to 900 nm in a microstructure fiber with a single cycle of holes around the fiber core, the core diameter 3 μm, and the length 1.5 m (curve *1*) and the spectrum of low-intensity Ti:sapphire-laser pulses transmitted through the same microstructure fiber with virtually no or very weak spectral broadening (curve *2*). (b) Cross-correlation traces for a pulse of the 720–900-nm spectral slice of supercontinuum (curve *1*) and a low-intensity Ti:sapphire-laser pulse transmitted through the same microstructure fiber with virtually no or very weak spectral broadening (curve *2*). Beam diagrams of (*1*) noncollinear sum-frequency generation (SFG) and (*2*) collinear second-harmonic generation (SHG) are also shown. The heights of the vertical bars represent the relative efficiencies of the SFG and SHG processes.

Sum-frequency and second-harmonic generation experiments performed with spectrally sliced supercontinuum radiation also allow the characteristic pulse duration to be estimated for different parts of the supercontinuum. Figure 16b presents the results of such cross-correlation experiments, where the intensity of the sum-frequency signal was measured as a function of the delay time between the fundamental radiation pulse of the Ti:sapphire laser and the broadband emission pulse coming out of the fiber and passing through a set of optical filters. Cross-correlation traces measured with the use of this approach were compared with the results of cross-correlation measurements performed in the same geometry for low-intensity Ti:sapphire-laser pulses transmitted through the microstructure fiber with virtually no or very weak spectral broadening (the spectrum of this signal is shown by curve *2* in Fig. 16a).

The cross-correlation trace measured for the broadband signal of the spectrally sliced supercontinuum (curve *1* in Fig. 16b) was much broader than the cross-correlation trace measured for the signal with virtually no or very weak spectral broadening (curve *2* in Fig. 16b). This comparison shows that different spectral components emitted as a part of the supercontinuum are characterized by different delay times. This effect is associated with the dispersion properties of microstructure-fiber-guided modes and can be employed to temporally and spatially resolve different frequency components in pump–supercontinuum probe experiments [124–126].

### 4.5 Mode structure and spectral properties of supercontinuum emission from microstructure fibers: concluding remarks

Thus, based on the investigation of the mode structure and spectral properties of supercontinuum radiation produced in microstructure fibers, a method of spatial filtering and spectral slicing of this supercontinuum radiation was proposed and experimentally implemented. The key physical effect behind this method of spatial and spectral filtering of supercontinuum radiation is associated with the increase in the separation between the propagation constants corresponding to adjacent guided modes with a decrease in the fiber core diameter. Microstructure fibers provide sufficiently small core diameters for the realization of this approach. Supercontinua in such fibers can be generated when multimode-phase-matched four-wave mixing results in a preferable generation of new spectral components emitted as a part of a supercontinuum in a certain (perhaps, high-order) guided mode.

The results of experimental studies presented in this section demonstrate the possibility of separating isolated spatial modes in supercontinuum radiation produced in such fibers within different spectral ranges. The proposed method of spatial mode filtering provides a high spatial quality of supercontinuum emission, which is sufficient to allow efficient further frequency conversion of spectrally sliced supercontinuum radiation. This frequency convertibil-

ity of supercontinuum spatial modes was demonstrated by experiments where spectrally sliced supercontinuum radiation was mixed with the fundamental radiation of a Ti:sapphire laser in a nonlinear crystal to produce the sum-frequency signal. The above-described method of spatial and spectral filtering of supercontinuum radiation from microstructure fibers opens the way to conveniently and efficiently employing microstructure-fiber-generated supercontinuum radiation for spectroscopic applications, time-resolved measurements, optical metrology, and coherence tomography, offering, at the same time, new solutions for the synthesis of ultrashort light pulses.

The studies described in this section have also demonstrated the possibility of achieving a high spectral quality of supercontinua produced in microstructure fibers. Supercontinuum-generating microstructure fibers thus offer new approaches to designing a new generation of optical parametric amplifiers and broadband radiation sources for spectroscopic, metrological, and biomedical applications.

## 5. Nonlinear-optical interactions of laser pulses in hollow photonic-crystal fibers

In this section, we explore the potential of hollow-core photonic-crystal fibers for the enhancement of nonlinear-optical processes. We will discuss the results of experiments on four-wave mixing of picosecond pulses and self-phase modulation of femtosecond laser pulses demonstrating a radical enhancement of nonlinear-optical phenomena in hollow PCFs relative to the regime of tight focusing and standard, solid-cladding hollow fibers.

### 5.1 Four-wave mixing in hollow-core photonic-crystal fibers

Four-wave mixing is one of the main classes of nonlinear-optical processes [92]. Interactions of this type are widely used for frequency conversion, control of ultrashort pulses, and spectroscopic applications. Waveguide regimes of laser-pulse propagation allow the efficiency of FWM processes to be substantially enhanced due to the radical increase in the length of nonlinear-optical interaction [2]. In particular, planar waveguides provide an unprecedented sensitivity level of coherent anti-Stokes Raman scattering, allowing the detection of the CARS signal from single molecules [85]. The sensitivity of FWM spectroscopy of gases can be substantially improved through the use of hollow waveguides [70 – 72]. The magnitude of optical losses in air-guided modes of hollow fibers rapidly (as $a^{-3}$) increases with a decrease in the inner radius $a$ of the fiber [73]. The FWM waveguide enhancement factor in hollow fibers (shown by curve *1* in Fig. 7a) is thus physically limited, with its limiting value being determined by the fiber core radius.

Hollow-core fibers with a microstructure or photonic-crystal (two-dimensionally periodic) cladding [38 – 40] (see Fig. 1d) allow the level of optical losses to be radically reduced with respect to conventional hollow fibers. Air-guided modes in such fibers are supported due to the high reflectivity of the periodic structure in the fiber cladding within the spectral ranges corresponding to photonic band gaps [38, 40]. Hollow photonic-crystal fibers thus offer a unique opportunity of implementing highly efficient nonlinear-optical interactions of air-guided modes with transverse sizes of several micrometers (see curves *2* and *3* in Fig. 7a and Section 2). Pioneering experimental studies into the nonlinear optics of microstructure fibers, carried out by Philip Russell's group at the University of Bath [41], have shown that such fibers allow the threshold of stimulated Raman scattering to be reduced to unprecedentedly low levels.

In this section, we will discuss the results of experiments demonstrating a radical enhancement of FWM in hollow photonic-crystal fibers. We will show that these fibers can provide an 800-fold enhancement of the FWM process $3\omega = 2\omega + 2\omega - \omega$ (where $\omega$ and $2\omega$ are the frequencies of fundamental radiation and the second harmonic of a picosecond Nd : YAG laser, respectively) relative to the regime of tight focusing.

Experiments on four-wave mixing [42] were performed with hollow-core photonic-crystal fibers having an inner diameter of about 14 μm and a period of the photonic-crystal cladding equal to 5 μm (see the insets in Fig. 17). Transmission spectra of these hollow-core photonic crystal fibers displayed characteristic well-pronounced peaks (Fig. 17). The origin of these peaks is associated with the high reflectivity of a periodically structured fiber cladding within photonic band gaps, which substantially reduces radiation losses in guided modes within narrow spectral ranges. Radiation with wavelengths falling outside the photonic band gaps of the cladding leaks from the hollow core. Such leaky radiation modes are characterized by high losses, giving virtually no contribution to the signal at the output of the fiber. Since the peaks in the transmission spectra of hollow-core photonic-crystal fibers are, in fact, maps of

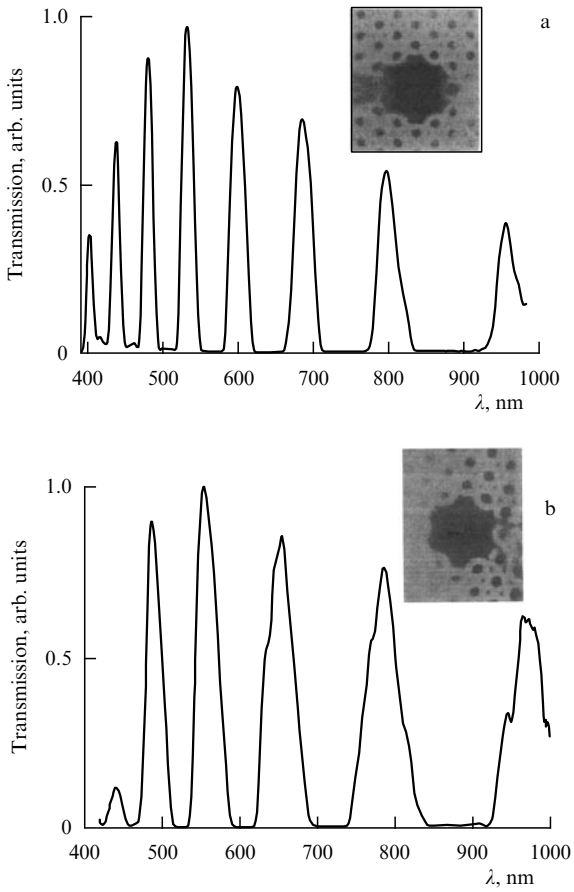


**Figure 17.** Transmission spectra measured for hollow-core photonic-crystal fibers with different cross-section geometries (shown in the insets). The period of the structure in the cladding is about 5 μm.

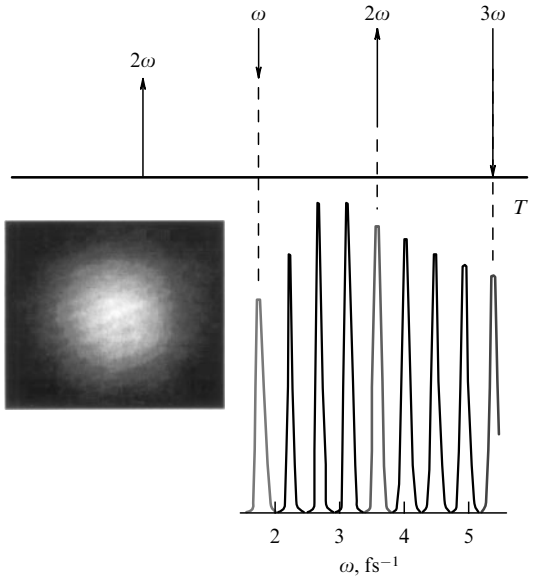


**Figure 18.** Diagram of the four-wave mixing process $3\omega = 2\omega + 2\omega - \omega$ (top) and the transmission spectrum of a hollow-core photonic-crystal fiber designed to simultaneously transmit the two-color pump (at 1.06 and 0.53 μm) and the FWM signal (bottom). The inset shows the transverse intensity distribution of second-harmonic pump radiation in the air-guided mode of the hollow-core photonic-crystal fiber.

photonic band gaps of their two-dimensionally periodic cladding, the spectra of air-guided modes in such fibers can be tuned by changing the fiber cladding structure.

Hollow-core photonic-crystal fibers employed in FWM experiments were designed in such a way as to provide maximum transmission simultaneously for the fundamental radiation of a Nd : YAG laser, as well as for its second and third harmonics. The diagram of the FWM process, resulting in the generation of a signal at the frequency of the third harmonic, and the transmission spectrum of the fiber are shown in Fig. 18. The magnitude of optical losses was estimated to be 0.09 $cm^{-1}$ at the wavelength of 1.06 μm and 0.08 $cm^{-1}$ at the wavelength of 0.532 μm for these fibers. The length of the fiber was chosen to be 9 cm, slightly less than the optimal length for the FWM process,

$$l_{\mathrm{FWM}} = \frac{\ln 3}{\alpha},$$

where $\alpha$ is the coefficient of optical losses, which is assumed to be approximately the same for all the frequencies involved in the FWM process. The expected FWM waveguide enhancement ratio, as can be seen from Fig. 7a, may be as high as 800 – 1000 under these conditions.

The experimental setup was based on a picosecond laser system, which generated two-color pump radiation for the FWM process at the wavelengths of 1.06 μm (pump radiation with the frequency $\omega$) and 0.53 μm (pump radiation with the frequency $2\omega$). The picosecond laser included a passively mode-locked Nd : YAG master oscillator with a negative-feedback-controlled cavity $Q$-factor, a single-pulse selection unit, and amplifying stages [127]. Passive mode locking in the master oscillator was implemented with the use of a saturable absorber film, which was placed in front of the rear cavity mirror. Negative feedback was introduced by inserting an electro-optical switch controlled with a fast-response photomultiplier inside the cavity. A similar electro-optical switch was used to select a single pulse from the train of pulses produced by the master oscillator. The energy of a single 30-ps laser pulse thus selected ranged from 30 to 40 μJ. The single-pulse selection unit also served as an optical decoupler, suppressing the parasitic feedback between the amplifying stages and the master oscillator and preventing radiation reflected from the optical elements of the amplification system from influencing the build-up of laser pulse trains in the master oscillator.

An amplified single pulse of 1.06-μm radiation was used to generate the second harmonic in a DKDP crystal (Fig. 19). The second-harmonic signal was separated from the fundamental beam with a dichroic mirror. The optical path lengths of the fundamental and second-harmonic pulses were matched with the use of an optical delay line. These beams were then brought together on a dichroic mirror and were coupled into a hollow-core photonic-crystal fiber placed on a three-dimensional translation stage (Fig. 19). The signal at the frequency of the third harmonic of the fundamental radiation, $3\omega$, can be produced in a hollow-core photonic-crystal fiber through both the $3\omega = 2\omega + 2\omega - \omega$ FWM process and the direct third-harmonic generation $3\omega = \omega + \omega + \omega$. Experiments performed with only the fundamental beam used as a pump have shown, however, that direct third-harmonic generation is much less efficient than two-color FWM.

Linearly polarized fundamental and second-harmonic pulses of Nd : YAG-laser radiation coupled into a hollow photonic-crystal fiber excited the fundamental waveguide modes. The inset in Fig. 18 shows a typical intensity distribution of second-harmonic pump radiation at the output of the fiber. The power of the FWM signal produced in a hollow photonic-crystal fiber was compared with the

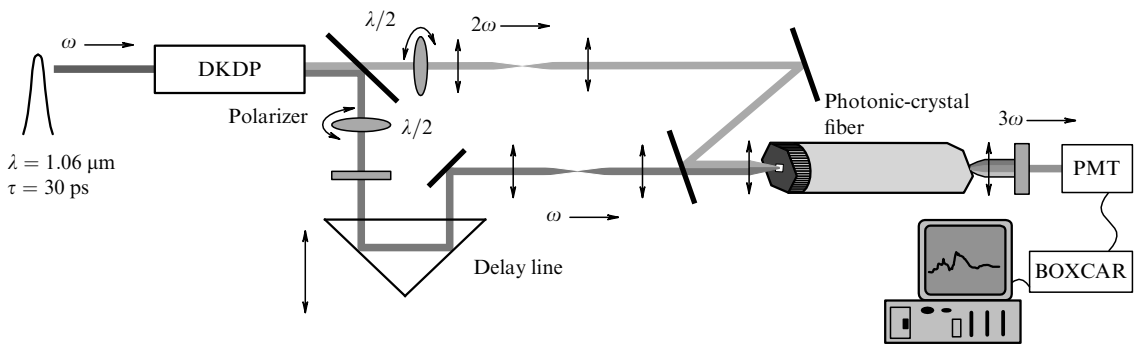


**Figure 19.** Experimental setup for the investigation of four-wave mixing in a hollow-core photonic-crystal fiber.

power of the FWM signal generated by tightly focused pump beams with the same wavelengths and the same energies. The FWM waveguide enhancement factor under the above-specified experimental conditions was estimated as approximately 800. This result qualitatively agrees with our theoretical analysis (cf. curves *2* and *5* in Fig. 7a). The FWM waveguide enhancement factor is limited by the optical losses of photonic-crystal fibers. We can expect, based on our calculations, that hollow-core photonic-crystal fibers with the magnitude of optical losses reduced down to 0.01 $cm^{-1}$ could enhance FWM processes by more than four orders of magnitude relative to the regime of tightly focused pump beams (curve *3* in Fig. 7a).

Table 2 compares the waveguide enhancement factor of the FWM process $3\omega = 2\omega + 2\omega - \omega$ attainable with a hollow-core photonic-crystal fiber to the waveguide enhancement achieved for the same FWM process in experiments with conventional, solid-cladding hollow fibers [128] using Nd : YAG-laser pulses with the same durations and frequencies. This comparison shows that hollow-core photonic-crystal fibers allow the FWM waveguide enhancement factor to be increased more than 50 times as compared with solid-cladding hollow fibers. The FWM signal can be reliably detected under conditions of the above-described experiments with microjoule picosecond pump pulses, i.e., at the level of pump energies unprecedentedly low for off-resonance FWM in the gas phase.

**Table 2.** Waveguide enhancement of four-wave mixing $3\omega = 2\omega + 2\omega - \omega$ of 30-ps pulses in hollow fibers with a solid and photonic-crystal cladding.

| Hollow fiber | $a$, μm | $L$, cm | $\mu$ | $E_\omega$, μJ | $E_{2\omega}$, μJ |
|---|---|---|---|---|---|
| solid cladding [128] | 100 | 10 | 15 | 10 | 10 |
| photonic-crystal cladding [42] | 13 | 9 | 800 | 2 | 2 |

*Notation*: $a$, inner diameter of a hollow fiber; $L$, fiber length; $\mu$, waveguide FWM enhancement relative to the regime of tight focusing; $E_\omega$, $E_{2\omega}$, typical energies of the pump pulses with frequencies $\omega$ and $2\omega$ generating a reliably detectable FWM signal; $\omega$, the frequency of fundamental Nd: YAG-laser radiation

### 5.2 Self-phase modulation of femtosecond pulses in hollow photonic-crystal fibers

Hollow fibers [73] are intensely used in modern laser systems to increase the length of nonlinear-optical interactions of laser pulses and to enhance nonlinear-optical processes [61]. Fibers of this type allow nonlinear-optical spectral transformations of ultrashort pulses to be implemented without a laser breakdown of the fiber core. Self-phase modulation in the gas filling the core of a hollow fiber makes it possible to produce pulses shorter than 5 fs [62, 63]. Stimulated Raman scattering of laser pulses in hollow fibers filled with Raman-active gases results in an efficient generation of multiple Raman sidebands. In the regime of locked phases, these Raman sidebands can be employed to synthesize pulses shorter than 4 fs [65]. Hollow fibers can radically enhance high-order harmonic generation [67 – 69] and improve the sensitivity of gas-phase analysis based on four-wave mixing spectroscopy [70 – 72].

The modes of standard hollow fibers with solid dielectric cladding are leaky (see Section 2), with the magnitude of optical losses for these modes increasing as $\lambda^2/a^3$ with a decrease in the radius $a$ of the hollow core ($\lambda$ is the radiation wavelength). There is no way, therefore, to use standard hollow fibers with very small inner diameters for laser experiments, which usually operate with hollow fibers with core diameters ranging from 100 to 500 μm. Such fibers are multimode, with higher-order modes having a significant influence on nonlinear-optical processes, as demonstrated by experiments on four-wave mixing [72, 129].

Optical losses of hollow fibers can be radically reduced if the fiber cladding has the form of a two-dimensionally periodic structure — photonic crystal. Photonic band gaps of the photonic-crystal cladding give rise to passbands in the transmission of a hollow fiber [38, 40]. Because of the finite bandwidth of photonic band gaps, the width of PCF passbands is also finite. This circumstance limits the duration of pulses that can be transmitted through such fibers, often leading to experimental difficulties in the transmission of femtosecond pulses.

Experiments [59] show the ways of matching the passbands of hollow PCFs with the parameters of ultrashort pulses. Below, we present the results of experiments devoted to the investigation of nonlinear-optical interactions of femtosecond pulses in hollow PCFs. Hollow PCFs providing a waveguide regime of nonlinear-optical interactions for femtosecond pulses of 800-nm radiation have been designed and fabricated. These experiments demonstrate a substantial enhancement of self-phase modulation of submicrojoule femtosecond Ti:sapphire-laser pulses in air-guided modes of PCFs.

The femtosecond laser system employed in the experiments [130] consisted of a Ti:sapphire master oscillator, a stretcher, a multipass amplifier, and a pulse compressor. The Ti: sapphire master oscillator was pumped by 4-W cw second-harmonic radiation of a diode-laser-pumped Nd:$YVO_4$ Verdi laser. The master oscillator generated laser pulses with a duration of 50 – 100 fs, a typical average output power up to 400 mW, and a pulse repetition rate of 100 MHz. Femtosecond pulses produced by the master oscillator were stretched up to 800 ps and launched into a multipass Ti: sapphire amplifier pumped with a nanosecond Nd:YAG laser with intracavity second-harmonic generation. Amplified 1-kHz picosecond chirped pulses were re-compressed to a duration of 100 – 130 fs in a single-grating pulse compressor. The energy of compressed laser pulses ranged up to 150 μJ. Self-phase modulation in hollow PCFs was studied with 100 – 120-fs pulses with an energy of 0.5 – 5 μJ.

Experiments [130] were performed with hollow-core PCFs having a period of the photonic-crystal cladding of about 5 μm and an inner diameter of approximately 14 μm (see the inset in Fig. 20a). Transmission spectra of these hollow-core PCFs displayed characteristic well-pronounced peaks (Fig. 20). The origin of these peaks is associated with the high reflectivity of a periodically structured fiber cladding within photonic band gaps, which substantially reduces radiation losses in guided modes within narrow spectral ranges. Radiation with wavelengths lying outside the photonic band gaps of the cladding leaks from the hollow core. Hollow-core photonic-crystal fibers providing minimum losses around the wavelength of 800 nm (Fig. 20) were designed and fabricated to guide femtosecond pulses of a Ti:sapphire laser. The length of PCFs used in experiments varied from 3 to 15 cm.

The figure of merit characterizing the waveguide enhancement of SPM in an optical fiber relative to the regime of a

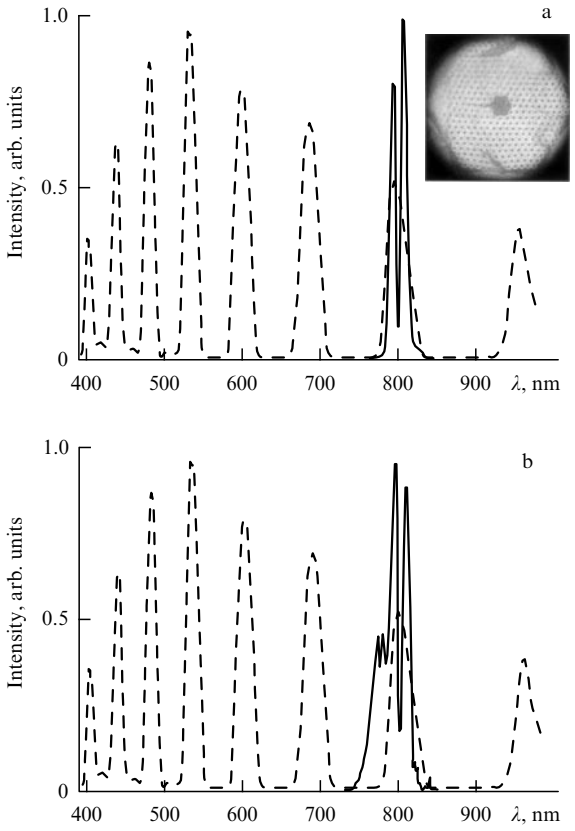


**Figure 20.** Solid lines show the spectra of laser pulses at the output of hollow photonic-crystal fibers with a length of 8 cm. The initial duration of 800-nm input pulses is 100 fs. The energy of radiation coupled into the fiber is 0.9 μJ (a) and 1.2 μJ (b). The dashed lines represent transmission spectra of photonic-crystal fibers. The inset in Fig. 20a displays a cross-section image of a photonic-crystal fiber with a period of the structure in the cladding of about 5 μm.

tightly focused laser beam scales as $\lambda/a^2\alpha$ with radiation wavelength $\lambda$, the magnitude of optical losses $\alpha$, and the fiber inner radius $a$. For a standard, solid-cladding hollow fiber, the magnitude of optical losses is given by Eqn (16). Due to the high reflectivity of a photonic-crystal cladding, hollow PCFs can substantially reduce optical losses as compared with conventional, solid-cladding fibers, where the magnitude of losses scales as $\lambda^2/a^3$.

Lower optical losses of PCFs allow a substantial increase in the figure of merit for self-phase modulation. This increase becomes especially noticeable in the case of hollow fibers with small core radii. Hollow PCFs with the core diameter $a \approx 14$ μm and the magnitude of optical losses $\alpha = 0.08$ cm$^{-1}$, employed in the experiments described in this section, increase the figure of merit for the SPM process by more than an order of magnitude relative to conventional, solid-cladding hollow fibers. Further increase in the waveguide figure of merit for the SPM process can be achieved by lowering optical losses of PCFs. Bouwmans et al. [131] have recently demonstrated hollow PCFs with the magnitude of radiation losses as low as 180 dB/km, suggesting ways for the further improvement of nonlinear-optical performance of hollow PCFs (see also Section 2).

Transmission of ultrashort pulses through hollow PCFs with minimum losses requires matching of the spectrum of laser pulses with the transmission spectrum of a PCF. The width of a passband in the transmission spectrum of a hollow PCF, controlled by the photonic band gap of the cladding, should be sufficient for the transmission of ultrashort laser pulses spectrally broadened due to self-phase modulation without considerable distortions of the pulse envelope.

Self-phase modulation in hollow PCFs was studied with the use of Ti:sapphire-laser pulses with an energy of 0.5 – 5 μJ and the initial duration 100 – 120 fs. These pulses were coupled into a hollow PCF with a core diameter of about 14 μm and the typical attenuation length estimated as approximately 11 cm. In view of radiation losses, the length of the PCF for SPM experiments was chosen to be 5 – 9 cm.

The solid line in Fig. 20 shows the spectra of radiation coming out of an 8-cm PCF. Pulses of 800-nm radiation with an initial duration of about 100 fs coupled into the fiber had an energy of 0.9 (Fig. 20a) and 1.2 μJ (Fig. 20b). The spectra of output pulses are broadened with respect to the input pulses due to self-phase modulation. Optimal conditions for the transmission of spectrally broadened pulses through the PCF are achieved when the spectrum of the pulse is matched with the relevant passband in the transmission of the PCF. Figure 20a shows an example of such optimal matching. The bandwidth of the SPM-broadened pulse presented in Fig. 20b exceeds the width of the PCF passband, which gives rise to additional radiation losses.

The bandwidth of the output pulse presented in Fig. 20a is approximately equal to 35 nm. The shape of the spectrum of this pulse corresponds to a nonlinear phase shift of about $1.5\pi$. Achieving similar levels of SPM broadening in standard, solid-cladding hollow fibers would typically require femtosecond pulses with intensities 40 to 100 times higher than the intensities of laser pulses employed in PCF experiments.

With an appropriate choice of the parameters of the laser pulse, the fiber, and the gas filling the fiber core, the SPM-broadened spectrum, as can be seen from Fig. 20a, can be matched with the transmission peak of the PCF. In the experiments described here, the PCF core was filled with atmospheric air with a typical nonlinear refractive index $n_2 \approx 5 \times 10^{-19}$ cm$^2$ W$^{-1}$ [132]. With the effective mode area estimated from the beam pattern at the output of the PCF as $S_{\text{eff}} \approx 70$ μm$^2$, the intensity of 0.8-μJ 100-fs laser pulses was $I \approx 9 \times 10^{12}$ W cm$^{-2}$.

For a PCF with a length of $L \approx 8$ cm, the elementary theory of SPM then predicts a spectral broadening

$$\Delta\lambda \approx 2n_2 \frac{I\lambda L}{\tau c} \approx 30 \text{ nm},$$

which agrees well with experimental results. Hollow PCFs thus provide a unique opportunity for implementing highly efficient nonlinear-optical interactions of air-guided modes of electromagnetic radiation with transverse sizes of a few micrometers in gas media.

### 5.3 Nonlinear optics of hollow photonic-crystal fibers: concluding remarks

The radical enhancement of FWM processes in hollow-core photonic-crystal fibers, demonstrated in this section, suggests new approaches for the nonlinear optics of high-power ultrashort laser pulses, high-field physics, and nonlinear spectroscopy. Hollow-core photonic-crystal fibers allow waveguide regimes of nonlinear-optical interactions to be implemented for high-power laser pulses that cannot be transmitted through standard fibers without irreversibly damaging these fibers.

Due to their capability of substantially enhancing nonlinear-optical processes and the possibility of tailoring the dispersion of guided modes by changing the fiber structure, hollow photonic-crystal fibers is an attractive way to improve the efficiency of ultrashort-pulse synthesis through multiple Raman sideband generation, which was demonstrated recently with the use of solid-cladding hollow fibers [65]. The enhancement of FWM processes in hollow photonic-crystal fibers also makes it possible to substantially improve the sensitivity of nonlinear-optical spectroscopy of the gas phase and to loosen the requirements to the energies of laser pulses in nonlinear spectroscopy.

Experiments presented in this section also demonstrate a radical enhancement of self-phase modulation of femtosecond laser pulses in hollow-core photonic-crystal fibers. Photonic-crystal fibers supporting waveguide regimes of nonlinear-optical interactions of femtosecond pulses with the maximum transmission at 800 nm have been designed and fabricated. Femtosecond pulses can be transmitted and spectrally broadened in a single-mode regime in such fibers. This regime of nonlinear-optical interactions reduces to minimum radiation losses related to the excitation of higher-order guided modes and can never be implemented with standard hollow fibers with a solid cladding. Hollow PCFs thus provide a unique opportunity to implement highly efficient nonlinear-optical interactions of air-guided modes of electromagnetic radiation with transverse sizes of a few micrometers in gas media. Self-phase modulation of submicrojoule pulses with an initial duration of about 100 fs under these conditions can give rise to nonlinear phase shifts of about $1.5\pi$.

## 6. Conclusion

We have shown in this review that, due to the strong confinement of laser radiation in guided modes, microstructure fibers are ideally suited for enhancing a broad class of nonlinear-optical interactions, including self- and cross-phase modulation, four-wave mixing, third-harmonic generation, and stimulated Raman scattering. Strong confinement of electromagnetic radiation and dispersion tunability of guided modes allow low-energy laser pulses, including unamplified pulses, to be employed for the generation of supercontinuum — radiation with a broad continuous spectrum. The spectral width of supercontinuum radiation produced in microstructure fibers can reach several octaves. Supercontinuum-generating microstructure fibers lead to revolutionary changes in optical metrology and are widely employed in laser biomedicine, spectroscopy, photochemistry, and ultrafast optics.

Dispersion control of guided modes in microstructure fibers offers new solutions to the phase-matching problem in nonlinear optics, allowing these fibers to be employed not only as sources of broadband emission but also as efficient frequency converters for ultrashort laser pulses. Arrays of submicron fused silica waveguide channels built into microstructure fibers have been shown to allow efficient generation of frequency-tunable anti-Stokes radiation with the use of subnanojoule femtosecond Ti:sapphire-laser pulses. The proposed and implemented architecture of microstructure fibers permits efficient multiplex frequency conversion of femtosecond Ti:sapphire- and Cr:forsterite-laser pulses to the spectral range that is of special interest for photochemical and photobiological applications, suggesting new solutions for femtosecond spectroscopy and the control of ultrafast processes in physics, chemistry, and biology.

The radical enhancement of FWM processes in hollow-core photonic-crystal fibers, demonstrated in this section, suggests new approaches for the nonlinear optics of high-power ultrashort laser pulses, high-field physics, and nonlinear spectroscopy. Photonic-crystal fibers supporting waveguide regimes of nonlinear-optical interactions of femtosecond pulses with the maximum transmission at 800 nm have been designed and fabricated. Thus, microstructure-fiber-based optical components for frequency conversion and nonlinear-optical spectral transformation of ultrashort pulses substantially enhance the capabilities of femtosecond laser systems, extending the applicability area of ultrashort laser pulses, including unamplified femtosecond pulses, to new fields of basic research, as well as numerous applications related to spectroscopy, telecommunication technologies, coherent and quantum control, ultrafast photonics, and laser biomedicine.

**Acknowledgments**

The material in this review is in many ways based on the results of research in the optics of microstructure fibers carried out in the Laboratory of Photonics and Nonlinear Spectroscopy, Chair of General Physics and Wave Processes, Physics Department, M V Lomonosov Moscow State University. I am cordially grateful to A B Fedotov and D A Sidorov-Biryukov for their precious cooperation, valuable help, and permanent support. I am sincerely thankful to A A Ivanov, D A Akimov, S O Konorov, A N Naumov, E E Serebryannikov, and M S Syrchin for fruitful collaboration and numerous discussions.

Much of the material presented in this review reflects the results of research performed and originally published in collaboration with prominent research groups and outstanding scientists in Russia and abroad — M V Alfimov (Center of Photochemistry, Russian Academy of Sciences), D von der Linde and A P Tarasevitch (University of Duisburg – Essen), V I Beloglazov, N B Skibina, and A V Shcherbakov (Institute of Technology and Equipment for Glass Structures, Saratov), Yu N Kondrat'ev, V S Shevandin, K V Dukel'skii, and A V Khokhlov (S I Vavilov State Optical Institute), P K Kashkarov and A A Podshivalov (M V Lomonosov Moscow State University), P Russell, J Knight, T Birks, and W Wadsworth (University of Bath), L A Mel'nikov (N G Chernyshevsky Saratov State University), R Miles (Princeton University), D Chorvat, D Chorvat Jr., and I Bugar (International Laser Center, Bratislava), W Kiefer and M Schmitt (Wuerzburg University), J Haus (University of Dayton), M Scalora (Redstone Arsenal, Huntsville University), S N Bagayev and V S Pivtsov (Institute of Laser Physics, Siberian Division, Russian Academy of Sciences), F Giammanco (University of Pisa), V B Smirnov (St. Petersburg State University), E Wintner (Technical University of Vienna), C Sibilia (La Sapienza University, Rome), and V V Yakovlev (University of Wisconsin – Milwaukee). I am cordially grateful to all of them for this fruitful collaboration.

This study was supported in part by the President of the Russian Federation Grant MD-42.2003.02, the Russian Foundation for Basic Research (projects nos. 03-02-16929 and 02-02-17098), and the Volkswagen Foundation (project I/76 869).

## References


1. Snyder A W, Love J D *Optical Waveguide Theory* (Science Paperbacks, 190) (London: Chapman and Hall, 1983)
2. Agrawal G P *Nonlinear Fiber Optics* (Boston: Academic Press, 1989)
3. Kaiser P V, Astle H W *Bell Syst. Tech. J.* **53** (1974)
4. Knight J C et al. *Opt. Lett.* **21** 1547 (1996)
5. Knight J C et al. *Science* **282** 1476 (1998)
6. Koch K W (Ed.) "Focus issue: photonic crystal fiber" *Opt. Express* **9** (13) (2001)
7. Bowden C M, Zheltikov A M (Eds) "Nonlinear optics of photonic crystals: feature issue" *J. Opt. Soc. Am. B* **19** (9) (2002)
8. Monro T M et al. *Opt. Lett.* **25** 206 (2000)
9. Fedotov A B et al. *Pis'ma Zh. Eksp. Teor. Fiz.* **71** 407 (2000) [*JETP Lett.* **71** 281 (2000)]; Alfimov M V et al. *Pis'ma Zh. Eksp. Teor. Fiz.* **71** 714 (2000) [*JETP Lett.* **71** 489 (2000)]; Zheltikov A M et al. *Zh. Eksp. Teor. Fiz.* **120** 570 (2001) [*JETP* **93** 499 (2001)]
10. Zheltikov A M *Usp. Fiz. Nauk* **170** 1203 (2000) [*Phys. Usp.* **43** 1125 (2000)]
11. Eggleton B et al. *Opt. Express* **9** 698 (2001)
12. Knight J C et al. *IEEE Photon. Technol. Lett.* **12** 807 (2000)
13. Reeves W H et al. *Opt. Express* **10** 609 (2002)
14. Broderick N G R et al. *Opt. Lett.* **24** 1395 (1999)
15. Fedotov A B et al. *Appl. Phys. B* **73** 181 (2001)
16. Naumov A N et al. *J. Opt. Soc. Am. B* **19** 2183 (2002)
17. Coen S et al. *Opt. Lett.* **26** 1356 (2001)
18. Coen S et al. *J. Opt. Soc. Am. B* **19** 753 (2002)
19. Fedotov A B et al. *Appl. Phys. B* **77** 313 (2003)
20. Akimov D A et al. *Opt. Lett.* **28** 1948 (2003)
21. Dudley J M et al. *Opt. Express* **10** 1215 (2002)
22. Ranka J K, Windeler R S, Stentz A J *Opt. Lett.* **25** 796 (2000)
23. Ranka J K, Windeler R S, Stentz A J *Opt. Lett.* **25** 25 (2000)
24. Wadsworth W J et al. *J. Opt. Soc. Am. B* **19** 2148 (2002)
25. Herrmann J et al. *Phys. Rev. Lett.* **88** 173901 (2002)
26. Zheltikov A M (Ed.) "Supercontinuum generation: special issue" *Appl. Phys. B* **77** (2/3) (2003)
27. Diddams S A et al. *Phys. Rev. Lett.* **84** 5102 (2000)
28. Jones D J et al. *Science* **288** 635 (2000)
29. Holzwarth R et al. *Phys. Rev. Lett.* **85** 2264 (2000)
30. Bagayev S N et al. *Laser Phys.* **11** 1270 (2001)
31. Udem Th et al. *Phys. Rev. Lett.* **86** 4996 (2001)
32. Hartl I et al. *Opt. Lett.* **26** 608 (2001)
33. Fedotov A B et al. *J. Raman Spectrosc.* **33** 887 (2002)
34. Konorov S O, Zheltikov A M *Opt. Express* **11** 2440 (2003)
35. Baltuka A, Fuji T, Kobayashi T *Opt. Lett.* **27** 1241 (2002)
36. Lakó S et al. *Appl. Phys. B* **76** 267 (2003)
37. Akimov D A et al. *Laser Phys.* **13** 1279 (2003)
38. Cregan R F et al. *Science* **285** 1537 (1999)
39. Knight J C, Russell P St J *Science* **296** 276 (2002)
40. Konorov S O et al. *Pis'ma Zh. Eksp. Teor. Fiz.* **76** 401 (2002) [*JETP Lett.* **76** 341 (2002)]
41. Benabid F et al. *Science* **298** 399 (2002)
42. Konorov S O, Fedotov A B, Zheltikov A M *Opt. Lett.* **28** 1448 (2003)
43. Konorov S O et al. *Kvantovaya Elektron.* (in press) (2004)
44. Benabid F, Knight J C, Russell P St J *Opt. Express* **10** 1195 (2002)
45. Konorov S O et al. *J. Phys. D: Appl. Phys.* **36** 1375 (2003)
46. Konorov S O et al. *Laser Phys.* **13** 1046 (2003)
47. Fedotov A B et al. *IEEE J. Sel. Top. Quantum Electron.* **8** 665 (2002)
48. Fedotov A B et al. *Appl. Phys. B* **75** 621 (2002)
49. Konorov S O et al. *Zh. Eksp. Teor. Fiz.* **123** 975 (2003) [*JETP* **96** 857 (2003)]
50. Dumais P et al. *Opt. Lett.* **18** 1996 (1993)
51. Birks T A, Wadsworth W J, Russell P St J *Opt. Lett.* **25** 1415 (2000)
52. Akimov D A et al. *Appl. Phys. B* **74** 307 (2002)
53. Akimov D A et al. *Kvantovaya Elektron.* **33** 317 (2003) [*Quantum Electron.* **33** 317 (2003)]
54. Akimov D A et al. *Pis'ma Zh. Eksp. Teor. Fiz.* **77** 9 (2003) [*JETP Lett.* **77** 7 (2003)]
55. Hartl I et al. *Opt. Lett.* **26** 608 (2001)
56. Harbold J et al., in *Conf. on Lasers and Electro-Optics* (*CLEO'2002*), *Long Beach, CA, May 19–24, 2002*, CTuU6
57. Benabid F, Knight J C, Russell P St J *Opt. Express* **10** 1195 (2002)
58. Naumov A N, Zheltikov A M *Kvantovaya Elektron.* **32** 129 (2002) [*Quantum Electron.* **32** 129 (2002)]
59. Konorov S O et al. *Laser Phys.* **13** 1170 (2003)
60. Fedotov A B et al. *J. Opt. Soc. Am. B* **19** 2156 (2002)
61. Zheltikov A M *Usp. Fiz. Nauk* **172** 743 (2002) [*Phys. Usp.* **45** 687 (2002)]
62. Nisoli M, de Silvestri S, Svelto O *Appl. Phys. Lett.* **68** 2793 (1996)
63. Nisoli M et al. *Opt. Lett.* **22** 522 (1997)
64. Duhr O et al. *Opt. Lett.* **24** 34 (1999)
65. Zhavoronkov N, Korn G *Phys. Rev. Lett.* **88** 203901 (2002)
66. Durfee C G III et al. *Opt. Lett.* **22** 1565 (1997)
67. Rundquist A et al. *Science* **280** 1412 (1998)
68. Tamaki Y, Midorikawa K, Obara M *Appl. Phys. B* **67** 59 (1998)
69. Constant E et al. *Phys. Rev. Lett.* **82** 1668 (1999)
70. Miles R B, Laufer G, Bjorklund G C *Appl. Phys. Lett.* **30** 417 (1977)
71. Fedotov A B et al. *Appl. Phys. B* **72** 575 (2001)
72. Naumov A N et al. *Pis'ma Zh. Eksp. Teor. Fiz.* **73** 301 (2001) [*JETP Lett.* **73** 263 (2001)]
73. Marcatili E A J, Schmeltzer R A *Bell Syst. Tech. J.* **43** 1783 (1964)
74. Adams M J *An Introduction to Optical Waveguides* (Chichester: Wiley, 1981)
75. Yariv A, Yeh P *Optical Waves in Crystals: Propagation and Control of Laser Radiation* (New York: Wiley, 1984)
76. Zheltikov A M, Naumov A N *Kvantovaya Electron.* **31** 471 (2001) [Quantum Electron. **31** 471 (2001)]
77. Akhmanov S A, Koroteev N I *Metody Nelineĭnoĭ Optiki v Spektroskopii Rasseyaniya Sveta: Aktivnaya Spektroskopiya Rasseyaniya Sveta* (Methods of Nonlinear Optics in Light Scattering Spectroscopy: Active Spectroscopy of Light Scattering) (Moscow: Nauka, 1981)
78. Eesley G L *Coherent Raman Spectroscopy* (Oxford: Pergamon Press, 1981)
79. Druet S A J, Taran J-P E *Prog. Quantum Electron.* **7** 1 (1981)
80. Eckbreth A C *Laser Diagnostics for Combustion Temperature and Species* (Energy and Engineering Science Ser., Vol. 7) (Cambridge, Mass.: Abacus Press, 1988)
81. Kiefer W *J. Mol. Struct.* **59** 305 (1980)
82. Zheltikov A M, Koroteev N I *Usp. Fiz. Nauk* **169** 385 (1999) [*Phys. Usp.* **42** 321 (1999)]
83. Stegeman G I et al. *Opt. Lett.* **8** 295 (1983)
84. de Boeij W P et al. *Appl. Spectrosc.* **47** 723 (1993)
85. Kanger J S, Otto C, Greve J *Appl. Spectrosc.* **49** 1326 (1995)
86. Konorov S O et al. *Pis'ma Zh. Eksp. Teor. Fiz.* **75** 74 (2002) [*JETP Lett.* **75** 66 (2002)]
87. Konorov S O et al. *J. Raman Spectrosc.* **33** 955 (2002)
88. Levenson M D, Song J J, in *Coherent Nonlinear Optics: Recent Advances* (Topics in Current Physics, Vol. 21, Eds M S Feld, V S Letokhov) (Berlin: Springer-Verlag, 1980) p. 293
89. Maker P D, Terhune R W *Phys. Rev.* **137** A801 (1965)
90. Broeng J et al. *Opt. Lett.* **25** 96 (2000)
91. Koroteev N I, Naumov A N, Zheltikov A M *Laser Phys.* **4** 1160 (1994)
92. Shen Y R *The Principles of Nonlinear Optics* (New York: J. Wiley, 1984)
93. Fejer M M et al. *IEEE J. Quantum Electron.* **28** 2631 (1992)
94. Byer R L *J. Nonlinear Opt. Phys. Mater.* **6** 549 (1997)
95. Scalora M et al. *Phys. Rev. A* **56** 3166 (1997)
96. Zheltikov A M, Tarasishin A V, Magnitskiĭ S A *Zh. Eksp. Teor. Fiz.* **117** 691 (2000) [*JETP* **91** 298 (2000)]
97. Dumeige Y et al. *Appl. Phys. Lett.* **78** 3021 (2001)
98. Akimov D A et al. *Appl. Phys. B* **77** 299 (2003)
99. Efimov A et al. *Opt. Express* **11** 910 (2003)
100. Konorov S O et al. *Laser Phys.* **13** 1170 (2003)
101. Zheltikov A M et al. *Kvantovaya Elektron.* **32** 542 (2002) [*Quantum Electron.* **32** 542 (2002)]
102. Zheltikov A M *Opt. Spektrosk.* **95** 440 (2003) [*Opt. Spectrosc.* **95** 410 (2003)]
103. Zheltikov A M *Zh. Eksp. Teor. Fiz.* **124** 558 (2003) [*JETP* **97** 505 (2003)]
104. Fedotov A B et al. *Laser Phys.* **13** 856 (2003)
105. Monro T M et al. *J. Lightwave Technol.* **17** 1093 (1999)
106. Monro T M et al. *Meas. Sci. Technol.* **12** 854 (2001)
107. Serebryannikov E E, Zheltikov A M *Laser Phys.* **13** 1339 (2003)

108. Iaconis C, Walmsley I A *IEEE J. Quantum Electron.* **35** 501 (1999)
109. Naumov A N, Zheltikov A M *Opt. Express* **10** 122 (2002)
110. Ivanov A A, Alfimov M V, Zheltikov A M *Laser Phys.* **10** 796 (2000)
111. Brown G H (Ed.) *Photochromism* (Techniques of Chemistry, Vol. 3) (New York: Wiley-Interscience, 1971)
112. Dürr H, Bouas-Laurent H (Eds) *Photochromism*: *Molecules and Systems* (Studies in Organic Chemistry, Vol. 40) (Amsterdam: Elsevier, 1990)
113. Barachevskiĭ V A, Lashkov G I, Tsekhomskiĭ V A *Fotokhromizm i Ego Primenenie* (Moscow: Khimiya, 1977)
114. Fritzsche J *CR Acad. Sci.* **69** 1035 (1867)
115. Parthenopoulos D A, Rentzepis P M *Science* **245** 843 (1989)
116. Akimov D A et al. *Jpn. J. Appl. Phys.* **36** 426 (1997)
117. Lecomte S et al. *Appl. Phys. Lett.* **77** 921 (2000)
118. Konorov S O et al. *Appl. Phys. B* **76** 707 (2003)
119. Cattaneo S et al. *J. Opt. Soc. Am. B* **19** 2032 (2002)
120. Willner I *Accounts Chem. Res.* **30** 347 (1997)
121. Alfano R R (Ed.) *The Supercontinuum Laser Source* (New York: Springer-Verlag, 1989)
122. Fedotov A B et al. *Laser Phys.* **13** (7) (2003)
123. Fedotov A B et al. *Zh. Eksp. Teor. Fiz.* **122** 986 (2002) [*JETP* **95** 851 (2002)]
124. Kovalenko S A et al. *Phys. Rev. A* **59** 2369 (1999)
125. Kovalenko S A et al. *Chem. Phys. Lett.* **323** 312 (2000)
126. Dobryakov A L et al. *Solid State Commun.* **116** 437 (2000)
127. Zheltikov A M, Koroteev N I, Fedotov A B *Laser Phys.* **4** 569 (1994)
128. Fedotov A B et al. *Laser Phys.* **11** 515 (2001)
129. Naumov A N et al. *Zh. Eksp. Teor. Fiz.* **120** 280 (2001) [*JETP* **93** 247 (2001)]
130. Konorov S O et al. *Laser Phys.* **14** (2004) (in press)
131. Bouwmans G et al. *Opt. Express* **11** 1613 (2003)
132. Marburger J H *Prog. Quantum Electron.* **4** 35 (1975)